A novel triptolide analog downregulates NF-κB and induces mitochondrial apoptosis pathways in human pancreatic cancer

Qiaomu Tian[1#], Peng Zhang[2#], Yihan Wang[1], Youhui Si[1], Dengping Yin[1], Christopher R Weber[3], Melissa L Fishel[4], Karen E Pollok[4], Bo Qiu[2], Fei Xiao[2], Anita S Chong[1*]

[1]Department of Surgery, The University of Chicago, Chicago, IL
[2]Cinkate Pharmaceutical Corp, ZhangJiang District, Shanghai
[3]Department of Pathology, The University of Chicago, Chicago, IL
[4]Department of Pediatrics, Indiana University, Indianapolis, IN

[#]These authors contributed equally

*To whom correspondence should be addressed:
Anita S. Chong, PhD
Professor, Section of Transplantation
Department of Surgery
The University of Chicago
5841 S. Maryland Ave
Chicago, IL60637
Email: achong@uchicago.edu
Tel: (773) 702-5521

Abstract

Background Pancreatic cancer is the seventh leading cause of cancer-related death worldwide, and despite advancements in disease management, the 5-year survival rates stands at only 9%. Triptolides have potent anti-tumor activity against different types of cancers, including pancreatic cancer, however poor solubility and toxicity limit their translation into clinical use.

Methods We synthesized a novel pro-drug of triptolide, (*E*)-19-[(1'-benzoyloxy-1'-phenyl)-methylidene]-Triptolide (CK21), and formulated into an emulsion for in vitro and in vivo testing in rats and mice, and using human pancreatic cancer cell lines and patient-derived pancreatic tumor organoids. A time-course transcriptomic profiling of tumor organoids treated with CK21 in vitro was conducted to define its mechanism of action, as well as transcriptomic profiling at a single time point post-CK21 administration in vivo.

Findings Intravenous administration of emulsified CK21 resulted in the stable release of triptolide, and potent anti-proliferative effects on human pancreatic cancer cell lines and patient-derived pancreatic tumor organoids *in vitro,* and with minimal toxicity *in vivo*. Time course transcriptomic profiling of tumor organoids treated with CK21 *in vitro* revealed <10 differentially expressed genes (DEGs) at 3 h and ~8,000 DEGs at 12 h. Overall inhibition of general RNA transcription was observed, and Ingenuity pathway analysis together with functional cellular assays confirmed inhibition of the NF-κB pathway, increased oxidative phosphorylation and mitochondrial dysfunction, leading ultimately to increased reactive oxygen species (ROS) production, reduced B-cell-lymphoma protein 2 (BCL2) expression, and mitochondrial-mediated tumor cell apoptosis.

Interpretation CK21 is a novel pro-drug of triptolide that exerts potent anti-proliferative effects on human pancreatic tumors by inhibiting the NF-κB pathway, leading ultimately to mitochondrial-mediated tumor cell apoptosis.

Funding The study of the anti-tumor efficacy of CK21 supported in part by a research grant from Cinkate Pharmaceutical Corp; the funders had no role in the study design, interpretation or decision to publish. Patient-derived pancreatic tumor organoids were a generous gift from the Organoid and Primary Culture Research Core at University of Chicago.

Key Words: Triptolide, pancreatic cancer, apoptosis

Introduction

Pancreatic cancer is the seventh leading cause of cancer related deaths globally and the third leading in the United States, and has the lowest 5-year survival rate (2-9%) among all the cancers[1]. Pancreatic ductal adenocarcinoma accounts for >90% of all pancreatic cancer cases, and poor outcomes have been attributed to late diagnoses when the cancer is at advance stages[2], where the majority of cases are accompanied with distant metastasis[3,4] and when most patients are not eligible for resection[5]. Fluorouracil, and gemcitabine are FDA approved as adjuvant chemotherapy after pancreatic cancer resection[6], FOLFIRINOX, Abraxane with gemcitabine represent first-line chemotherapy for patients with metastatic pancreatic cancer[7-9]. For patients with resectable disease followed by adjuvant chemotherapy, anticipated median overall survival Is 54.4 months, however, for patients with advanced unresectable disease, the survival benefit with multiagent chemotherapy is only 2-6 months[2].

The Chinese herb, *Tripterygium wilfordii* hook F (Thunder God vine), has anti-inflammatory, immunosuppressive, contraceptive, and anti-tumor activities, and has been used for centuries as traditional Chinese medicine for treating rheumatoid arthritis and lupus. In 1972, Morris *et al*. extracted triptolide from *T. wilfordii* and characterized it as a structurally unique diterpene triepoxide, with potential anti-leukemic properties[10]. Subsequently, triptolide was shown to have anti-tumor effects in pre-clinical mouse models of breast cancer[11,12], cholangiocarcinoma[13], osteosarcoma[14], lung cancer[15,16], acute myeloid leukemia[17,18], ovarian cancer[19,20], prostate cancer[21], gastric cancer[22], colon cancer[23], and pancreatic cancer[24,25]. Multiple mechanisms have been proposed for triptolide-induced antitumor activity, including inhibition of NF-κB[26], and HSP70[27]. Notably, Titov *et al*. reported that triptolide binds covalently to human XPB (ERCC3) and inhibits its DNA-dependent ATPase activity, leading to the inhibition of RNA polymerase II-mediated transcription and nucleotide excision

repair[28]. However, it is unclear how this non-specific inhibition of an essential transcription factor could exert selectivity against tumors.

While triptolide is a promising anti-cancer drug, poor solubility and toxicity have limited its clinical development, and a number of analogs of triptolide have been developed for improved clinical performance[29,30]. In Phase I clinical studies, a soluble analog PG490-88/F60008[31] resulted in significant toxicity and had high interindividual variability in pharmacokinetic studies, thus stopping further development. Minnelide[32] is another analog with superior solubility and potent anti-tumor 1activity in multiple preclinical cancer models. Phase I clinical trial (ClinicalTrials.gov Identifier: NCT03129139) showed significant activity in highly refractory metastatic pancreatic cancer, and it is currently in a Phase II open label trial (ClinicalTrials.gov ID NCT03117920).

In this study, we synthesized a novel pro-drug of triptolide, CK21, by decorating the C-19 with a C-C double bond to generate (*E*)-19-[(1'-benzoyloxy-1'-phenyl)-methylidene]-Triptolide, formulated it into an emulsion, and investigated its efficacy and mode of action. We report that CK21 inhibited the *in vitro* proliferation of multiple pancreatic cancer cell lines, was effective at eliminating large pancreatic tumors in heterotopic and orthotopic xenograft animal models with minimal toxicity, and confirmed the efficacy of CK21 against multiple patient-derived pancreatic tumor organoids *in vitro* and *in vivo*. We performed transcriptome analysis on the pancreatic organoid response to CK21 *in vitro*, and on the *in vivo* response of pancreatic tumors to CK21. We identified that CK21 reducing overall transcription, inhibited the NF-κB pathway, induced mitochondria dysfunction, and ultimately, mitochondrial-mediated apoptosis was identified as the likely mechanism for the anti-tumor activity of CK21.

Methods

Study design overview

We synthesized a novel pro-drug of triptolide, CK21, and formulated it into an emulsion. We tested the efficacy of CK21 *in vitro* using cell proliferation assays and multiple pancreatic cancer cell lines, and in vivo in heterotopic and orthotopic xenograft mouse models. We also tested the efficacy of CK21 against multiple patient-derived pancreatic tumor organoids *in vitro* and *in vivo*. We performed transcriptome analysis on the pancreatic organoid response to CK21 *in vitro*, and on the *in vivo* response of pancreatic tumors to CK21. This analysis identified the ability of CK21 to reduce overall transcription, inhibit the NF-κB pathway, induce mitochondria dysfunction, and ultimately, mitochondrial-mediated apoptosis. We confirmed inhibition of NF-κB expression and translocation in pancreatic cell lines using imaging flow cytometry, Western blotting and RT-PCR.

Ethics statement and study approval

All animal experiments were approved by the Institutional Animal Care and Use Committee at the University of Chicago, and adhered to the standards of the NIH Guide for the Care and Use of Laboratory Animals. Pancreatic tumors from patients with pancreatic ductal adenocarcinoma were collected under University of Chicago IRB12-1108 and IRB13-1149.

Reagents

Human pancreatic tumor cell lines were obtained from commercial sources. Human tumor organoids were obtained from patients with pancreatic ductal adenocarcinoma, confirmed to be tumor based on pathologic assessment, and developed into organoid culture according to established protocols[39]. Luciferase-transfected AsPC-1 tumors[34], and mouse tumors from genetically KPC mice that spontaneously develop pancreatic cancer[47] have been previously described. CK21 was synthesized as described below. All other reagents listed in the Key Resources Table were validated by the manufacturer.

Synthesis and formulation of CK21

Under nitrogen protection, a mixture of triptolide (1.8 g, 5 mmol) and anhydrous tetrahydrofuran (250 mL) was cooled to -20 °C, and lithium 2,2,6,6-tetramethylpiperidine in tetrahydrofuran/toluene (7.5 mL, 2.0M, 15 mmol) was added dropwise. After stirring for 30 min, benzoyl chloride (1.05 mL, 7.5 mmol) was added dropwise and reacted for 1 h, followed again with benzoyl chloride (7.5 mmol) and reacted for another 2 h. The reaction was quenched by adding aqueous sodium carbonate (10%), and the mixture was extracted with ethyl acetate (250 mL×3). The organic phases were combined, dried over anhydrous sodium sulfate, and concentrated under reduced pressure. The crude product was separated and purified by silica gel chromatography (dichloromethane: ethyl acetate = 2:1), and the target product (white solid, 2.55 g, yield 90%) was collected and further recrystallized in a mixed organic solvent (dichloromethane/hexane) to obtain a final product (2.13 g, yield 85%, purity >99% by UPLC).

CK21 was dissolved in medium chain triglycerides (MCT) at 90°C under nitrogen. PC-98T, DSPE-MPEG2000 and glycerol were dissolved in water to form the water phase. The oil phase was dispersed at room temperature in the water phase with high-speed shear mixing (FAS90-22, FLUKO) at 2,800 rpm for 30 min. The pH was adjusted to 4-7, and volume was made up to 100% with water. The final emulsion was obtained by high-pressure homogenization using microfluidizer (M-7125-20K, MFIC) at 10,000 psi for one cycle and at 18,000 psi for two cycles. Finally, the emulsion was sealed in vials (5 mL: 1.5 mg) after flushing with nitrogen gas and autoclaved at 121°C for 15 min.

Characterization of CK21 compound

1H NMR (Bruker, 400MHz, CDCl3): δ 8.25 (dd, J = 1.6 Hz, 8.0 Hz, 2H), 7.76 (dd, J = 1.6 Hz, 8.4 Hz, 2H), 7.67 (m, 1H), 7.58 (t, J = 7.2 Hz, 2H), 7.43~7.38 (m, 3H), 3.80 (d, J = 3.2 Hz, 1H), 3.39 (d, J = 2.8 Hz, 1H), 2.98 (d, J = 10 Hz, 1H), 2.75~2.69 (m, 1H), 2.63~2.58 (m, 1H), 2.56 (d, J = 6.4 Hz, 1H), 2.53 (d, J = 10 Hz, 1H), 2.40~2.32 (m, 2H), 2.21~2.14 (m, 1H), 1.88 (dd, J = 14.0 Hz, 13.2 Hz, 1H), 1.55~1.52 (m, 1H), 1.18~1.11 (m, 1H), 1.15 (s, 3H), 0.92 (d, J = 7.2 Hz, 3H), 0.82 (d, J = 6.8 Hz,

3H); 13C NMR (Bruker, 100 MHz, CDCl3): δ168.1, 164.5, 150.3, 142.2, 134.4, 133.5, 131.9, 130.5, 129.9,129.2, 128.9, 128.6, 128.1, 128.0, 72.8, 65.8, 65.3, 60.7, 60.0, 56.5, 53.7, 40.7, 36.7, 29.3, 27.9, 24.6, 17.8, 17.6, 16.7, 15.0.

Mass Spectrometry (AGILENT, ESI+): Calculated for C34H32O8[M]: 568.62, found 569.22 $[M^+H]^+$ and 591.21 $[M^+Na]^+$.

CK21 crystals were obtained by careful evaporation of a mixture of CK21 in combined solvent of dichloromethane and hexane at room temperature. A crystal with size of 0.10×0.03×0.02 mm was chosen to be scanned at X-ray diffraction. Data collection was carried out using a Bruker D8 Venture diffractometer with graphite mono-chromated Ga Kα radiation (λ = 1.34139 Å) at 296 K. Structures were solved by direct methods using the SHELXS program and refined with the SHELXL program (Bruker).

Pharmacokinetic study of CK21

CK21 emulsion (0.3 mg/mL) was injected intravenously into fasted SD rats at a dose of 3 mg/kg for males and 1.5 mg/kg for females. At designed timepoints, 60 μL blood samples were collected, protein precipitated and centrifuged at 13000 rpm for 10 min, 4°C. 5 μL of the supernatant was injected for LC-MS/MS (Q-Trap 6500) analysis. The PK data were calculated using Phoenix WinNonlin 6.3.

Human pancreatic cancer cell lines and organoids

Human pancreatic cancer cell line, AsPC-1, was cultured in RPMI with 10% fetal bovine serum (FBS), 1% L- Glutamine, and 1% penicillin streptomycin(P/S). Panc-1 was cultured in DMEM with 10% FBS and 1% P/S. Both AsPC-1 and Panc-1 were purchased from ATCC.

Pancreatic tumors from patients with pancreatic ductal adenocarcinoma were collected under IRB12-1108 and IRB13-1149, confirmed to be tumor based on pathologic assessment, and developed into organoid culture according to established protocols[39]. Four different organoids, U0118-8, U049MAI, U114SOK, and U123M15-T, were investigated. For the optimal culture, derived

organoids were embedded in growth factor reduced Matrigel and cultured in Intesticult^{TM} complete media, supplemented with A83-01, fibroblast growth factor 10, gastrin I, N-acetyl-L-cysteine, nicotinamide, and B27 supplement, primocin. Tocris Y-27632 dihydrochloride, a selective p160 ROCK inhibitor, was added when thawing the organoids[39].

In vitro proliferation assay

AsPC-1, Panc-1 and tumor organoids were seeded in 96-well plates and cultured with the indicated concentrations of CK21, or Gemcitabine. CK21 was prepared by dissolving in DMSO and diluting with PBS. At selected times, 20 μL of CellTiter 96® AQueous One solution was added into the 96-well plate, and then incubated at 37°C for 2 hours. The absorbance was read at 490 nm using Spectra Max® i3X (Molecular Devices).

Mice and xenograft

All animal work that described in this study were approved by the Institutional Animal Care and Use Committee (ACUP72467, ACUP72527). Female or male athymic nude-Foxn1^{nu} mice age from 6 to 8 weeks were purchased from Envigo. AsPC-1 or Panc-1 cells were subcutaneously implanted in the scruff of a nude mice at 5×10^6 cells/mice. Mice were treated with different dosages of CK21 daily by intraperitoneal injection. Blank emulsion was provided to the no treatment group. Gemcitabine was also provided to mice at 75 mg/kg once a week as a positive control. The effect of CK21 with another human pancreatic tumor cell line, Panc-1, was also evaluated in the subcutaneous model. The U049MAI organoid was used to test the efficacy of CK21 in the same way.

Tumor size was recorded weekly and calculated by $1/2\times L\times W^2$. L was the length of the tumor; W was the width of the tumor. Weight of mice were monitored once a week. At the end of the experiment, mice were sacrificed by cervical dislocation. Liver, kidney, pancreas, as well as tumor tissue were harvested and fixed in 10% formalin. Haemotoxylin and Eosin (H&E), terminal deoxynucleotidyl transferase dUTP nick end labeling (TUNEL) staining were performed on respective

tissues. All the slides were scanned using ScanScope XT slide scanner and analyzed using Aperio eSlideManager.

Orthotopic Tumor Model with Transfected AsPC-1

Luciferase-transfected AsPC-1[34] (1×10^6 /mouse) was injected into the tail of the pancreas, and one week of tumor implantation, CK21 was provided at 3 mg/kg daily for the treatment group. In the no treatment group, blank emulsion was provided. During the four weeks of treatment, mice were administrated with D-luciferin (Perkin Elmer) and subjected to Xenogen bioluminescence imaging weekly.

Immunomodulation of CK21 at a spontaneous rejection mice model

Murine pancreatic cancer cell lines were derived from KPC mice, which are spontaneously developing pancreatic cancer[47]. KPC-960 were developed from KPC mice with a mixed background of B6×129, and were subcutaneously implanted into female, naïve B6×129 mice at 5×10^6 cells/mice. After spontaneous rejection, mice were rested for 2 weeks and then challenged with KPC-960 cells at 5×10^6 cells/mice. A dosage of 3 mg/kg of CK21 was provided daily starting at day 5 or day 7. For evaluation of CK21 on memory response, mice that rejected the tumors without any CK21 treatment were rested for 2 weeks and then received a second tumor challenge and 3 mg/kg of CK21 daily, starting at day 3.

Mice that rejected the KPC-960 tumor were sacrificed, splenocytes were collected and ex-vivo specific cytotoxic assay performed. Specifically, target cells KPC-960 and negative control KC-6141 were labeled at 10:1 concentration of carboxyfluorescein succinimidyl ester (CFSE) respectively. Two cell lines were then mix at 1:1 ratio and cultured with harvested splenocytes at 1:1, 1:5, 1:10, 1:20, and 1:50 ratios. After overnight co-culture, cells were subjected to flow cytometry (BD™ LSR II) to quantify relative cytotoxicity

Transcriptome analysis of CK21 treated patient-derived organoids

Two organoids, U049MAI, U123M15-T, were cultured with CK21 at 50 nM for 3 hours, 6 hours, 9 hours and 12 hours. Total RNA was extracted using a RNeasy® Plus Mini Kit (Qiagen), and total RNA quantified using the 2100 Bioanalyzer (Agilent). Samples with a RIN >8 was outsourced to Novogene for library construction and sequencing (Illumina Platform (PE150)) with 20 M raw reads/sample. The reads were mapped to the Homosapien genome (GRCh38) using STAR software with ≥95% mapping rate. Differential expression analysis was performed using DESeq2 package in R[64]. Molecular and cellular function analysis and pathway enrichment was analyzed using Ingenuine Pathway Analysis software (Qiagen). Duplicate samples were prepared for each condition.

In vivo RNA seq was also performed on orthotropic, luciferase-transfected AsPC-1 tumors. Specifically, luciferase transfected AsPC-1 was implanted into pancreas, and after one week, mice were treated with CK21 at 3 mg/kg for 3 days. Tumor tissues were then resected and RNA seq was performed. Quadruplicate samples were prepared for each condition.

Imaging Flow cytometry

AsPC-1, Panc-1 were cultured with 50 nM CK21 for 24 hours and 48 hours. Cells were fixed with 4% paraformaldehyde, and incubated overnight in cocktail of antibody (DPAI, anti-p65) containing 0.1% Triton X-100. Stained cells were subjected to imaging flow cytometry (Amnis® ImageStream®^{X}Mk II) and images analyzed using IDEAS^{R} software. Specifically, the 'Similarity' feature in IDEAS^{R} indicates the spatial relationship between the p65 and nuclei. Low similarity scores exhibit a predominant cytoplasmic distribution of p65, whereas high similarity scores indicate a predominant nuclear distribution of p65.

Western blotting

AsPC-1, Panc-1, U049MAI, or U123M15-T were cultured with 50 nM CK21 for 24 hours. Cells then were collected, washed, and lysate for 10 min on ice. Protein concentration of each sample was detected following the protocol of Pierce™ Detergent Compatible Bradford Assay. Total of 20 µg denatured protein was then loaded into each lane of NuPAGE™ Bis-Tris Gel and run using Mini Gel

Tank (Invitrogen). Gels were transferred to 0.45 µm Invitrolon™ PVDF membrane using Mini Blot Module (Invitrogen). Membranes were blocked in 5% BSA overnight at 4°C. Membranes were then incubated overnight at 4°C with primary antibodies, including anti-DDIT4, anti-BCL2, anti-Caspase3, or anti-ß-actin. Secondary goat anti-rabbit H&L IgG (HRP) was then incubated for one hour at room temperature. Finally, the chemiluminescent signal was enhanced by with SuperSignal™ West Pico PLUS Chemiluminescent Substrate, and protein expression was detected using Azure™ Biosystems 600.

RT-qPCR

Predesigned primers were purchased from Integrated DNA Technologies, which included XBP1 (Hs.PT.58.1903847), GADD45B (Hs.PT.58.19897476.gs), MYC (Hs.PT.58.26770695), GUSB (Hs.PT.58v.27737538), VAMP1 (Hs.PT.58.26743095), POLR2A (Hs.PT.58.14390640), XIAP (Hs.PT.56a.23056448), DDIT4 (Hs.PT.58.38843854.g), ACTB (Hs.PT.56a.19461448.g) for human tumor organoid samples. DDIT4 (Mm.PT.58.43159110.g), GUSB (Mm.PT.39a.22214848), MYC (Mm.PT.58.13590978), GADD45B (Mm.PT.58.10699383.g), ACTB (Mm.PT.39a.22214843.g), XIAP (Mm.PT.56a.5536843), XBP1 (Mm.PT.58.30961962) for mouse pancreatic tumor cell line samples.

U049MAI or U123M15-T were cultured with 50 nM CK21 for 24 hours, total RNA was extracted with an RNeasy® Plus Mini Kit (Qiagen) and quantified using Nanodrop 1000 spectrophotometer (Thermo Fisher). RNA of each sample was reverse transcribed into cDNA using High capacity cDNA reverse transcription kit (Applied Biosystems). RT-qPCR were run on QuantStudio 3 (Applied Biosystems) using PowerUp™ SYBR™ green master mix with specific primers. RT-qPCR of murine pancreatic cancer cell lines, KC-6141 and KPC-961, were prepared in the same way.

Statistical analysis

Data are presented as means ± standard error (SEM). Statistical analyses were performed using GraphPad Prism software. Differences between groups were analyzed using unpaired t-tests, one-way or two-way ANOVA with post-hoc tests, as indicated in the figure legends.

Results

Novel modified triptolide, CK21, show improved pharmacokinetics

We designed a new modification strategy to triptolide to generate CK21, by decorating the C-19 with a C-C double bond to generate (*E*)-19-[(1'-benzoyloxy-1'-phenyl)-methylidene]-Triptolide (Fig1.a). Briefly, a mixture of triptolide (1.8 g, 5 mmol) with anhydrous tetrahydrofuran (250 mL) was kept at -25°C~-20°C under nitrogen protection. Benzoyl chloride (1.05 mL, 7.5 mmol) and Lithium 2,2,6,6-tetramethylpiperidine in tetrahydrofuran/toluene (7.5mL, 2.0M, 15mmol) were then added dropwise to produce an intermediate compound, IM464. After 1 h, addition of benzoyl chloride and lithium 2,2,6,6-tetramethylpiperidine was repeated, and the reaction was quenched by adding aqueous sodium carbonate (6%). Following concentration under reduced pressure, the crude product was separated and purified by silica gel chromatography, and the target product collected and further recrystallized in methylene chloride/hexane to obtain CK21 that was used in the *in vitro* studies. Using ^{1}H NMR, ^{13}C NMR and mass spectrometry, we confirmed the structure of CK21, and the absolute configuration of CK21 was established by single crystal X-ray diffraction (Fig1.b). We then formulated CK21 with medium chain triglycerides, phospholipids, glycerol, and DSPE-MPEG2000 (Fig1.c) to produce a CK21 emulsion (Fig1.d) that was used in the *in vivo* studies.

To examine the conversion of CK21 into triptolide *in vivo*, and to establish pharmacokinetics and to avoid toxicity, we intravenously administrated 3 mg/kg or 1.5 mg/kg CK21 into Sprague Dawley male or female rats, and the concentration of CK21 and triptolide in the plasma quantified. CK21 had a $T_{1/2}$ of 1.3 h and 0.225 h for male and female rats respectively. Released triptolide reached T_{max} at 0.25 and 0.75 h with a C_{max} of 78.3 and 81.9 nM respectively for male and female rats. A stable release of triptolide 30 nM to 80 nM was observed for up to 2 hours (Fig.1e), and we hypothesized may mitigate the toxicity observed with other triptolide derivatives, which exhibit a spike release[31]. Finally, we observed that *in vitro* incubation of the human pancreatic cancer cell lines,

AsPC-1, and Panc-1, with CK21 at 5-100 nM for 24, 48 and 72 h resulted in a dose-and time-dependent inhibition of cell proliferation (Fig.1f).

A comparison of CK21 and triptolide (TP) revealed that they had similar IC50 (μM) when tested in vitro using a cell viability assay with different cancer cell lines and human fibroblasts (Fig.s1). However, the in vivo toxicity of TP in mice was significantly higher than CK21 in vivo (supplement Fig.s2).

CK21 inhibits AsPC-1 and Panc-1 proliferation *in vitro* and tumor growth *in vivo*

To evaluate the efficacy of CK21 pro-drug *in vivo*, we developed a xenograft model where AsPC-1 tumors were subcutaneously implanted into female nude mice (Fig.2a). Daily treatment with CK21 at all doses tested (1.25, 2.5, 3 and 5 mg/kg) significantly inhibited AsPC-1 tumor growth (Fig.2c). Higher dosages of CK21 at 3 mg/kg or 5 mg/kg daily completely eliminated the tumor after 28 days of treatment (Fig.2b). After 28 days of CK21 treatment, no mice demonstrated tumor relapse during the subsequent 6-month follow-up observation (supplement Fig.s3).

No significant weight loss was detected when female mice were treated with ≤ 3 mg/kg CK21, compared to the control (no treatment) group (Fig.2d). In contrast, mice exhibited severe weight loss with 5 mg/kg CK21. To further confirm the lack of toxicity of CK21 (3 mg/kg), we performed H&E and TUNEL staining to detect cell apoptosis on the kidney, liver, and pancreas of mice after 28 days treatment. We observed no toxicity in the kidney, liver, and pancreas tissues after 28 days of treatment (Fig.2e); in contrast, after 14 days of CK21 treatment, AsPC-1 tumors showed a 5-fold increase of TUNEL-positive staining compared to the no Rx group (Figs.2f&g). Thus, we concluded that CK21 given at 3 mg/kg daily exhibited high efficacy and minimal toxicity, and this dose was employed for the remaining of study. In a second subcutaneous xenograft model with the Panc-1

tumor cell line, 3 mg/kg daily of CK21 also resulted in significant inhibition of tumor growth (supplement Fig.s4).

Orthotopic tumor mouse models are generally preferred over heterotopic subcutaneously-located pancreatic tumors because they offer tissue site-specific pathology, allow studies of metastasis, and are deemed more clinically relevant[33], while the development of pancreatic tumors expressing luciferase/fluorescent proteins has facilitated the longitudinal monitoring of orthotopically located pancreatic tumors[34]. We next evaluated the efficacy of CK21 in an orthotropic xenograft model, using luciferase-transfected AsPC-1 implanted into the pancreas of nude mice and allowing the tumor to develop for 1-2 weeks before initiating CK21 treatment. The presence and size of the tumor were monitored weekly by quantifying the bioluminescence intensity (Fig.2h), and overall, a 10 to 15-fold reduction in bioluminescence intensity was observed in mice that received CK21 compared to untreated controls (Fig.1i). In addition, no mice died in the CK21 treatment group, whereas 5 out of 11 animals were sacrificed in the no Rx group due to the large tumor size while the experiment was ongoing (Fig.2j). Finally, we noted that while most of the untreated mice develop metastatic disease by the end of the experiment (Fig.2h), the CK21 treated mice did not.

Delayed CK21 therapy inhibits growth of tumors that escaped earlier therapies

The mortality of pancreatic tumors is often due to late detection when the tumor is at an advanced stage. To evaluate the efficacy of CK21 against late-stage tumors, CK21 treatment was initiated only after subcutaneous AsPC-1 tumors reached a large size of ~900 mm^2 (Fig.3a). Despite this delay in the initiation of treatment, CK21 was able to completely reduce the size of AsPC-1 tumors after 28 days of treatment, with all mice showing a significant response (Fig.3b).

Gemcitabine is a standard of care medication for pancreatic cancer in the clinic[2], therefore we next tested whether gemcitabine in combination with CK21 might offer improved efficacy. We treated mice for 4 weeks with suboptimal doses of CK21 (3 mg/kg, 3 days/wk) and gemcitabine (25 mg/kg, 3 days/wk), with each drug given on alternate days to avoid toxicity (Fig.3c). The combination therapy

did not show improved inhibition of AsPC-1 growth compared to CK21 monotherapy (Fig.3d), and indeed failed to induce complete regression of AsPC-1 tumors. In mice where tumors were detectable after 28 days treatment with CK21 or gemcitabine monotherapy, or combination therapy, we tested whether switching to CK21 (3 mg/kg) daily treatment (Fig.3e) was able to induce tumor regression. We observed that irrespective of whether mice failed CK21 (3x/wk) or gemcitabine monotherapy, or combination therapy, switching to daily CK21 monotherapy for 28 days induced significant tumor regression (Fig.3e).

Transcriptome analysis of patient-derived organoids revealed early down-regulation of DDIT4 and XBP1 by CK21

It is now recognized that 3-D patient-derived organoids offer a better recapitulation of the heterogeneous, architectural, morphologic and genetic features of patient pancreatic tumor, compared to long-term established 2-D monolayer cell lines[35-38]. We therefore investigated four organoids derived from different pancreatic cancer patients[39], UC12-0118-8, U049MAI, U123SOK, and U123M15-T, and tested the susceptibility to CK21 *in vitro* and *in vivo*. Details of the origin, mutations of these organoids were described in supplement Fig.s5. We observed that 72 hours of *in vitro* incubation with CK21 (25 nM) significantly inhibited UC12-0118-8, U049MAI, and U123SOK growth, and CK21 (50 nM) significantly inhibited proliferation of all four organoids (Fig.4a). In addition, we were able to propagate U049MAI as a slower-growing subcutaneous tumor in nude mice. Treatment with CK21 (3 mg/kg, daily) for 28 days, also significantly reduced U049MAI tumor growth compared to the untreated control group (Fig.4b).

Because pancreatic tumor organoids better preserve the genetic signatures than pancreatic tumor cell lines, we performed a time-course RNA-seq of U049MAI and U123M15-T treated with CK21 for 3, 6, 9 and 12 hours. We hypothesized that the early time points might reveal the initiating mechanism of action that result ultimately in the control of tumor growth; indeed, the number of differentially expressed genes (DEGs) significantly increased with prolonged CK21 treatment, from

less than 10 DEGs at 3 h up to 8,000 DEGs at 12 h (Fig.4c & Supplement Fig.s6). We identified the genes that were differentially expressed at early time points and continuously upregulated or downregulated at later time points (Fig.4d), and confirmed with qPCR, of a significant downregulation of DDIT4, MYC, XBP1 and XIAP, as well as a significant upregulation of POLR2A, GADD45 and VAMP1(Fig.4e). We also performed transcriptome analysis on the AsPC-1 tumor, orthotopically implanted in the pancreas for 7 days and then treated by CK21 for three days. CK21 induced a similar DEG expression profile as *in vitro* treated organoids, with downregulated DDIT4 and XBP1, as well as upregulated POLR2A (Fig.4g).

DDIT4 was one of the genes consistently and strongly downregulated by CK21 in both organoids and AsPC-1, with significant effects observed as early as 3 hours of CK21 treatment *in vitro* and at day 3 *in vivo*. At the protein level, we also observed a significant decrease of DDIT4 expression after CK21 treatment of 24 hours (Supplement Fig.s7). Interestingly, DDIT4 has been identified as a prognosis marker and highly expressed in pancreatic tumors[40], prompting the investigation into whether DDIT4 inhibition might be the triggering mechanism of action and thus serve as a predictive biomarker for CK21 sensitivity. However, knock-down of DDIT4 in Panc-1 only induced very modest *in vitro* susceptibility to CK21, and the overexpression of DDIT4 in AsPC-1 didn't result a difference to CK21 response (Supplement Fig.s8). Furthermore, in two mouse pancreatic tumor cell lines derived from genetically modified KC or KPC mice that were only modestly sensitive to CK21 treatment (Supplement Fig.s9), DDIT4 as well as other early responder genes showed strong alterations in expression profiles comparable to tumors that were more sensitive to CK21 (Supplement Fig.s10). Therefore, these early responder genes are not likely to be essential mediators leading to tumor susceptibility to CK21.

Ingenuity pathway analysis of patient-derived organoids reveal down-regulation of the NF-κB signaling pathway by CK21

At the later timepoint of 12 h after CK21 treatment, both U049MAI and U123M15-T had over 8,000 DEGs compared to the no Rx group (Figs.5a&b). We then used Ingenuity pathway analysis (IPA, Qiagen) on the DEGs to identify the major molecular and cellular functions that were significantly affected by CK21 treatment (Fig.5c). First, CK21 treatment was predicted to inhibit RNA and DNA transcription, expression of RNA, and transactivation of RNA transcription in both organoids; this observation corroborates a previous report on the ability of triptolide to inhibit RNA transcription[28]. In addition, DEGs induced by CK21 were enriched for inhibition of cell proliferation and cell survival, and for inducing apoptosis and tumor cell necrosis. These observations collectively are consistent with TUNEL-positive staining of ASPC-1 with CK21 treatment *in vivo*, and support the conclusion that induction of cell apoptosis is the mechanism for the anti-tumor activity of CK21.

We used IPA pathway enrichment analysis to further identify the canonical signaling/metabolic pathways regulated by CK21 that might lead to tumor cell apoptosis (Figs.5d&e). Interestingly, in both organoids, EIF2 signaling, oxidative phosphorylation and mitochondrial dysfunction were the major pathways highly upregulated by CK21, whereas the NF-κB, TGF-ß and telomerase signaling pathways were significantly downregulated at the 12 h treatment timepoint. In addition, at 9-hour timepoint, NF-κB was already significantly downregulated and oxidative phosphorylation as well as EIF2 signaling pathway were significantly upregulated (supplement Fig.s11). Collectively, these observations suggest that CK21 may be inhibiting NF-κB activity and inducing mitochondrial-mediated tumor cell apoptosis.

CK21 inhibits expression of NF-κB p65 and translocation to nuclei

NF-κB plays a major role in the regulation of immune, inflammatory response and cell proliferation[41]. In normal cells, NF-κB is activated by appropriate stimuli and then returns to its inactive state. In tumor cells, particularly in pancreatic cancer cells, NF-κB becomes constitutively activated and has an anti-apoptotic function[42,43]. After 12 h treatment with CK21, the genes (CHUK,

IKBKB and RELA) encoding the key regulators of the NF-κB pathway, IKKα, IKKβ and p65, were significantly downregulated in both organoids (Fig.6a).

To confirm the transcriptional findings that CK21 downregulates the NF-κB pathway, we stained the nuclei and p65 of AsPC-1 and Panc-1 with different fluorophores to visually determine their cellular location; similarity in the spatial localization between p65 and nuclei represents the translocation of NF-κB to nuclei (Fig.6b). In the no Rx group, p65 staining had a high similarity with nuclei staining, corresponding with constitutive nuclear localization of NF-κB in pancreatic cancer cells. After treatment with CK21 for 24 or 48 hours, both cell lines exhibited significantly lower expression of p65, consistent with RNA-seq analysis (Fig.6c). In addition, we observed reduced similarity of p65 and nuclei, indicating significantly reduced translocation of NF-κB to the nuclei in the presence of CK21 (Figs.6d&e). Taken together, the data demonstrate that CK21 inhibits NF-κB expression and translocation, which we hypothesize results in increased susceptibility tumor cell apoptosis.

CK21 induces reactive oxidative species and mitochondrial mediated apoptosis

The expression of genes encoding five mitochondrial respiratory chain complexes were significantly increased in pancreatic tumor organoids treated with CK21(Fig.6f), consistent with dysregulated mitochondrial function and increased susceptibility to mitochondrial-mediated apoptosis[44]. Because mitochondrial mediated apoptosis is often stimulated by oxidative stress, we first tested whether CK21 induced reactive oxidative species (ROS) in AsPC-1 and Panc-1 pancreatic tumor cell lines. In both cell lines, a trend towards an increase in ROS was observed as early as 8 hours after CK21 treatment, and a significant increase in ROS generation after 24 hours of culture with CK21 (Fig.6g). These observations raise the possibility that increased ROS production may trigger mitochondrial outer membrane permeabilization and release of pro-apoptotic mitochondrial proteins into the cytoplasm[44].

The B-cell-lymphoma protein 2 (BCL2) family of proteins play critical roles in regulating the mitochondrial pathway of apoptosis, and BCL2 functions as a critical anti-apoptotic survival protein[45]. To test whether BCL2 protein is reduced in CK21-treated cells, we quantified BCL2 protein expression by Western blotting. We observed that BCL2 was significant decreased in both AsPC-1 and Panc-1 cell lines, and in U049MAI, after 24 hours of CK21 culture (Fig.6h).

Because most apoptotic pathways lead to the activation of cysteine-dependent aspartate-specific proteases, and ultimately to cleaved effector caspases such as caspases-3, -6 and -7[45], we probed for cleaved caspase-3 in pancreatic tumors incubated with CK21. For Panc-1 and both pancreatic tumor organoids, cleaved caspase-3 was detected after 24 hours of culture with CK21 (Fig.6i) by Western blotting. We also confirmed increased caspase-3/7 in Panc-1 by flow cytometry (supplement Fig.s12). Interesting, cleaved caspase-3/7 was not detected in AsPC-1 after CK21 treatment, suggesting that apoptosis of these tumor cells may be explained by the involvement of other effector caspases or proteases. Collectively, these data point to CK21 downregulating the NF-kB pathway, promoting ROS production and mitochondrial-mediated tumor cell apoptosis.

CK21 showed minimal immunosuppression in a spontaneous tumor rejection model

A number of studies have reported on the immunosuppressive activity of triptolide[46], thus raising the potential concern that CK21 may inhibit the development of anti-tumor immune responses and prevent long-term tumor control. Indeed, although the analyses were conducted on CK21 treated tumor cells, IPA analysis indicated that CK21 inhibited lymphopoiesis, leukopoiesis and T cell development, consistent with potential immunosuppressive activity. To address this concern, we utilized a mouse KPC-960 pancreatic ductal-like tumor model derived from pancreatic tumors that spontaneously arose in KPC ($Kras^{G12D/+}Trp53^{R172H/+}$Pdx1-Cre) B6.129 mice[47] (Fig.7a). Upon subcutaneous implantation into B6.129 immunocompetent hosts, KPC-960 grew to a maximum tumor size by day 7 and then approximately 70% KPC-960 tumors were spontaneously rejected by day 14-17 post-implantation (Fig.7b). This contrasted with tumor formation in similar B6.129 host in Torres et

al. [47], we speculate that rejection of the KPC-960 tumor may be driven increased number of passages that resulted in the accumulation of mutations and/or to antigenic drift in the B6.129 hosts. To test whether CK21 could prevent the spontaneous regression of KPC-960, CK21 (3 mg/kg daily) therapy was initiated on day 5 or 7 post-implantation. We observed no statistically significant inhibition of tumor regression when CK21 treatment was started on day 5 or 6 post-implantation (Figs.7c&d) suggesting that the immunosuppressive activity of CK21 on established primary immune responses is minimal. The reason for the resistance to CK21 is not known and is the subject of future investigations.

In mice that cleared KPC-960 tumors were rested for 2 weeks without treatment and then challenged with a second KPC-960 tumor (Fig.7a); a more rapid tumor clearance was observed (Fig.7e). When CK21 treatment was initiated on day 3 of second tumor implantation, no significant change in the kinetics of tumor regression was observed compared to untreated controls (Fig.7f). In addition, mice that rejected the first KPC-960 tumors while receiving CK21 were rested and re-challenged with a second KPC-960 tumor. All the mice, including that did not receive CK21, were able to reject the tumor completely (Fig.7g). These observations further demonstrate CK21 did not inhibit the development of memory or recall anti-tumor responses.

Finally, to evaluate the quality of tumor-specific T cells after CK21 treatment, we performed an *ex vivo* tumor killing assay. Splenocytes were harvested from untreated mice that had rejected tumors, or mice that had received CK21-treatment after 1° or 2° tumor implantation and cultured with KPC-960 or a control KPC-6141 tumor *ex vivo* (Fig.7h). Splenocytes from mice treated with CK21 exhibited comparable killing of KPC-960 as splenocytes from untreated mice (Fig.7i). Collectively these data suggest that despite potent anti-tumor activity, CK21 was minimally immunosuppressive.

Discussion

Toxicity is the key challenge for using triptolide and its derivatives for its use as an anti-tumor agent in the clinic. Hepatotoxicity, reproductive toxicity, and nephrotoxicity have been identified as the major side effects for triptolide[48]. In addition, sex differences have been observed, where the female rats showed more toxicity under the same dosage of triptolide[49]. Cytochrome P450s (CYP) is essential for the metabolism of triptolide and CYP3A2, a male-predominant form in rats, may contribute to the sex-related differences[50]. Similar sex differences were also observed for CK21, where half the dose of CK21 in female rats had a similar triptolide exposure in plasma as male rats (Fig.1e), and the maximum tolerated dose (MTD) of CK21 was 3 mg/kg/dose for female rats and 6 mg/kg/dose for male rats (supplement Fig.s13). Consistent with the MTD of CK21 being different for male/female rats, we observed comparable efficacy of CK21 at 3 mg/kg in female mice (Fig.2c), and at 1.5 mg/kg in male mice (supplement Fig.s14). Whether these sex difference in triptolide metabolism will affect dosing in the clinic will have to be investigated in Phase I clinical trials. Nevertheless, despite sex difference, stable exposure of triptolide upon conversion from CK21 resulted in significantly mitigated toxicity, compared to other analogs such as F60008 that showed a steep release of triptolide which, we speculate, would lead to triptolide overexposure and severe toxicity observed in Phase 1 trials[31]. Another triptolide analog, MRx102 had a MTD of 3 mg/kg/dose for the female rats and 4.5 mg/kg/dose for the male rats[51]. Under the pharmacokinetic profile of CK21, we were able to dose the female athymic nude mice up to 5 mg/kg/day for 28 days with tolerable weight loss (Fig.2d), and at 3 mg/kg/day, where CK21 showed potent efficacy and no obvious toxicity (Figs.2c-e).

We used rigorous time-course transcriptomic profiling of pancreatic tumors response to CK21 to identify its mechanism of action on patient-derived pancreatic tumor organoids. Overall, the effect of CK21 corresponded to the major reported anti-tumor functions of triptolide, namely transcription inhibition and apoptosis induction. Triptolide was reported by Tivov *et al*. to covalently bind to XPB, a

subunit of the transcription factor TFIIH, resulting in the inhibition of its DNA-dependent ATPase activity, RNA polymerase II (Pol II)-mediated transcription and likely nucleotide excision repair[28]. Chen *et al*. further confirmed that triptolide functioned as a XPB/TFIIH inhibitor to limit promoter-proximal Pol II transcription initiation, resulting in decreased Pol II levels as early as 2 hours of treatment[52]. Likewise, our transcriptome analyses revealed broad downregulation of transcription and transactivation of RNA after 12 h CK21 treatment (Fig.5c). Furthermore, as early as 6 h of treatment, we observed a significant downregulation of a number of critical transcription factors, including XBP1 and ZNF628 (Fig.4d), which may mediate the broad inhibition of RNA and DNA transcription, as well as of RNA transactivation and expression observed at 12 h post-CK21 treatment (Fig.5c). Inhibition of RNA transcription and blockade of RNA synthesis can potentially lead to programmed cell death. For example, Santo *et al*. used a cyclin-dependent kinase inhibitor to inhibit Pol II phosphorylation and observed induction of apoptosis in myeloma cells[53]. Cai *et al*. also suggested inhibition of Pol II expression and phosphorylation resulted reduced expression of Mcl-1 and X-linked inhibitors of apoptosis (XIAP)[54]. Similarly, Carter *et al*. reported that tumor cell apoptosis induced by triptolide was accompanied by decrease of XIAP levels[18]. Consistent with Carter *et al*. we also observed a significant decrease of XIAP expression after CK21 treatment of two human pancreatic organoids *in vitro*, and of orthotopically transplanted AsPC-1 tumors *in vivo* (Figs.4d, f, g).

Our analysis of enriched signaling/metabolic pathways (Figs.5d&e) predicted the downstream effects of CK21's inhibition of general transcription that might lead to tumor cell apoptosis. As a potential consequence of transcription inhibition, genes for the key regulators of NF-κB pathway, such as CHUK, IKBKB and RELA, were significantly downregulated in both organoids (Fig.6a&supplement Fig.s13). We also observed decreased p65 expression on a protein level and reduced translocation of the NF-κB complex to the nucleus (Figs.6b-e). Therefore, activation of the NF-κB pathway was significantly inhibited after treatment with CK21. In addition to promoting cell proliferation and immune responses[41], NF-κB also plays a role in controlling mitochondrial dynamics and cell apoptosis[55].

Pazarentzos *et al*. demonstrated the localization of IκBα on the outer membrane of mitochondrial functions to inhibit apoptosis, especially in the tumor cells[56]. Liu *et al*. indicated the inhibition of NF-κB alone can induce the release of cytochrome C from mitochondria[57]. In our study, we observed a significant downregulation of NFKBIA, which encodes IκBα, in both organoids after CK21 treatment (Fig.6a& supplement Fig.s15). In addition, we also observed that the expression of genes encoding five mitochondrial respiratory chain complexes was significantly increased in pancreatic tumor organoids treated with CK21(Fig.6f). Collectively these data suggest a downstream effect of CK21 is promotion of dysregulated mitochondrial function and subsequently, increased susceptibility to mitochondrial-mediated intrinsic apoptosis[44].

As upstream regulators, BCL2 family proteins that reside or congregate on the surface of mitochondria govern cell-intrinsic apoptosis[58]. BCL2 family proteins have opposing functions: BCL2 is anti-apoptotic and promotes cell proliferation[59] whereas BAX is pro-apoptotic[60]. Under CK21 treatment, BCL2 expression in pancreatic cancer cells was significantly reduced (Fig.6h). Similar observations were reported in leukemic cells[18] and melanoma cells[61] after treated with triptolide. The expression of BCL2 and BAX regulates the equilibrium of mitochondrial membrane potential[62,63], thus CK21 may tip such equilibrium towards permeabilization and release of apoptogenic molecules into cytoplasm[63]. Eventually, effector caspases, such as caspase 3, 6, and 7, are cleaved and activated to induce apoptosis. In our study, we observed a significant increase of cleaved caspase 3 for Panc-1 and both pancreatic tumor organoids (Fig.6i). Finally, we noted subtle differences in the extent to which Bcl2 is inhibited and Caspase 3 is activated following CK21 treatment of the two pancreatic tumor cell lines and two patient-derived organoids; these observations underscore the notion that broad inhibition of RNA transcription allows CK21 to leverage distinct vulnerabilities and pathways to achieve apoptosis in different tumor cells.

Taken together, our study describes the development of a novel modified triptolide, CK21, with improved pharmacokinetics, and efficacy for pancreatic tumor cell lines and patient-derived

pancreatic tumor organoids. Transcriptomic profiling of the organoids and verification of protein expression collectively point to the induction of tumor cell apoptosis by CK21 is mediated by the inhibition of general transcription, leading to downstream effects involving NF-κB inhibition and mitochondria dysfunction.

Contributors

QT designed and performed the majority of experiments, and YW performed additional reviewer-requested experiments. YS assisted with RNA extraction for transcriptome analysis. DY performed some of the initial *in vivo* experiments and survival surgeries on the orthotopic mouse models. MLF and KEP generated and provided luciferase transfected AsPC-1. CRW provided patient-derived pancreatic tumor organoids and reviewed histology slides. PZ, BQ and FX oversaw the synthesis, characterization, PK studies of CK21, and comparison of CK21 with triptolide. PZ, XF, QT and ASC verified the underlying data. QT generated the figures, performed bioinformatics and statistical analyses of the data and wrote the paper. ASC and XF conceived the project, and ASC designed the experiments and co-wrote the paper. All authors read, commented and approved on the manuscript.

Declaration of Interests

PZ and BQ were employees of Cinkate Pharmaceutical Corp. PZ and FX (CEO of Cinkate Pharmaceutical Corp) are listed as inventors on Patent WO2018/019301A1, which covers the design and use of CK21 for pancreatic cancer. ASC received consulting fees from Cinkate Pharmaceutical Corp. No conflicts of interest, financial or otherwise, are declared by the other authors.

Acknowledgements

This research was supported in part by a research grant (to University of Chicago) from the Cinkate Pharmaceutical Corp. We thank the Organoid and Primary Culture Research Core at University of Chicago for the gift of patient-derived pancreatic tumor organoids, the Human Tissue Resource at University of Chicago for tissue processing and staining, the Cytometry and Antibody Technology Core for advising on flow cytometry and the Animal Resources Center at University of Chicago for mouse husbandry services. Dr. Surinder K. Bartra (University of Nebraska Medical Center) provided the mouse pancreatic tumor cell lines. Dr. Barbara Bailey and Dr. Helmut Hanenberg contributed to the generation of the luciferase transfected AsPc-1. We also gratefully acknowledge Dr. Mary

Buschman and Ms. Kori Kirby for advising on organoid culture, Stephanie Shen for advising on Western blotting, and Karin Peterson for training on mouse handling.

Data sharing statement

All data associated with this study are in the article or the Supplementary Materials. RNA-seq data will be available on request from the corresponding author, and are deposited in NCBI GEO under GSE225011.

References

1. Siegel RL, Miller KD, Jemal A. Cancer statistics, 2019. *CA: A Cancer Journal for Clinicians* 2019; **69**(1): 7-34.
2. Kamisawa T, Wood LD, Itoi T, Takaori K. Pancreatic cancer. *The Lancet* 2016; **388**(10039): 73-85.
3. Yachida S, Jones S, Bozic I, et al. Distant metastasis occurs late during the genetic evolution of pancreatic cancer. *Nature* 2010; **467**(7319): 1114-7.
4. Sohn TA, Yeo CJ, Cameron JL, et al. Resected adenocarcinoma of the pancreas-616 patients: results, outcomes, and prognostic indicators. *J Gastrointest Surg* 2000; **4**(6): 567-79.
5. Bilimoria KY, Bentrem DJ, Ko CY, Stewart AK, Winchester DP, Talamonti MS. National Failure to Operate on Early Stage Pancreatic Cancer. *Annals of Surgery* 2007; **246**(2): 173-80.
6. Oettle H, Neuhaus P, Hochhaus A, et al. Adjuvant Chemotherapy With Gemcitabine and Long-term Outcomes Among Patients With Resected Pancreatic Cancer. *JAMA* 2013; **310**(14): 1473.
7. Burris HA, 3rd, Moore MJ, Andersen J, et al. Improvements in survival and clinical benefit with gemcitabine as first-line therapy for patients with advanced pancreas cancer: a randomized trial. *J Clin Oncol* 1997; **15**(6): 2403-13.
8. Von Hoff DD, Ervin T, Arena FP, et al. Increased survival in pancreatic cancer with nab-paclitaxel plus gemcitabine. *N Engl J Med* 2013; **369**(18): 1691-703.
9. Conroy T, Desseigne F, Ychou M, et al. FOLFIRINOX versus gemcitabine for metastatic pancreatic cancer. *N Engl J Med* 2011; **364**(19): 1817-25.
10. Kupchan SM, Court WA, Dailey RG, Gilmore CJ, Bryan RF. Tumor inhibitors. LXXIV. Triptolide and tripdiolide, novel antileukemic diterpenoid triepoxides from Tripterygium wilfordii. *Journal of the American Chemical Society* 1972; **94**(20): 7194-5.

11. He J, Peng T, Peng Y, et al. Molecularly Engineering Triptolide with Aptamers for High Specificity and Cytotoxicity for Triple-Negative Breast Cancer. *Journal of the American Chemical Society* 2020; **142**(6): 2699-703.
12. Li J, Liu R, Yang Y, et al. Triptolide-induced in vitro and in vivo cytotoxicity in human breast cancer stem cells and primary breast cancer cells. *Oncology Reports* 2014; **31**(5): 2181-6.
13. Liu Q. Triptolide and its expanding multiple pharmacological functions. *International Immunopharmacology* 2011; **11**(3): 377-83.
14. Jiang C, Fang X, Zhang H, et al. Triptolide inhibits the growth of osteosarcoma by regulating microRNA-181a via targeting PTEN gene in vivo and vitro. *Tumor Biology* 2017; **39**(4): 101042831769755.
15. Reno TA, Kim JY, Raz DJ. Triptolide Inhibits Lung Cancer Cell Migration, Invasion, and Metastasis. *The Annals of Thoracic Surgery* 2015; **100**(5): 1817-25.
16. Song JM, Molla K, Anandharaj A, et al. Triptolide suppresses the in vitro and in vivo growth of lung cancer cells by targeting hyaluronan-CD44/RHAMM signaling. *Oncotarget* 2017; **8**(16): 26927-40.
17. Carter BZ, Mak DH, Shi Y, et al. MRx102, a triptolide derivative, has potent antileukemic activity in vitro and in a murine model of AML. *Leukemia* 2012; **26**(3): 443-50.
18. Carter BZ, Mak DH, Schober WD, et al. Triptolide induces caspase-dependent cell death mediated via the mitochondrial pathway in leukemic cells. *Blood* 2006; **108**(2): 630-7.
19. Hu H, Luo L, Liu F, et al. Anti-cancer and Sensibilisation Effect of Triptolide on Human Epithelial Ovarian Cancer. *Journal of Cancer* 2016; **7**(14): 2093-9.
20. Zhao H, Yang Z, Wang X, et al. Triptolide inhibits ovarian cancer cell invasion by repression of matrix metalloproteinase 7 and 19 and upregulation of E-cadherin. *Experimental & Molecular Medicine* 2012; **44**(11): 633.

21. Huang W, He T, Chai C, et al. Triptolide Inhibits the Proliferation of Prostate Cancer Cells and Down-Regulates SUMO-Specific Protease 1 Expression. *PLoS ONE* 2012; **7**(5): e37693.
22. Yang S, Chen J, Guo Z, et al. Triptolide inhibits the growth and metastasis of solid tumors. *Mol Cancer Ther* 2003; **2**(1): 65-72.
23. Wang Z, Jin H, Xu R, Mei Q, Fan D. Triptolide downregulates Rac1 and the JAK/STAT3 pathway and inhibits colitis-related colon cancer progression. *Experimental and Molecular Medicine* 2009; **41**(10): 717.
24. Chugh R, Sangwan V, Patil SP, et al. A Preclinical Evaluation of Minnelide as a Therapeutic Agent Against Pancreatic Cancer. *Science Translational Medicine* 2012; **4**(156): 156ra39-ra1.
25. Wang W, Li X, Sun W, et al. Triptolide triggers the apoptosis of pancreatic cancer cells via the downregulation of Decoy receptor 3 expression. *Journal of Cancer Research and Clinical Oncology* 2012; **138**(9): 1597-605.
26. Lee KY, Park JS, Jee YK, Rosen GD. Triptolide sensitizes lung cancer cells to TNF-related apoptosis-inducing ligand (TRAIL)-induced apoptosis by inhibition of NF-kappaB activation. *Exp Mol Med* 2002; **34**(6): 462-8.
27. Phillips PA, Dudeja V, McCarroll JA, et al. Triptolide Induces Pancreatic Cancer Cell Death via Inhibition of Heat Shock Protein 70. *Cancer Research* 2007; **67**(19): 9407-16.
28. Titov DV, Gilman B, He Q-L, et al. XPB, a subunit of TFIIH, is a target of the natural product triptolide. *Nature Chemical Biology* 2011; **7**(3): 182-8.
29. Noel P, Von Hoff DD, Saluja AK, Velagapudi M, Borazanci E, Han H. Triptolide and Its Derivatives as Cancer Therapies. *Trends in Pharmacological Sciences* 2019; **40**(5): 327-41.
30. Tong L, Zhao Q, Datan E, et al. Triptolide: reflections on two decades of research and prospects for the future. *Nat Prod Rep* 2021; **38**(4): 843-60.

31. Kitzen JJEM, De Jonge MJA, Lamers CHJ, et al. Phase I dose-escalation study of F60008, a novel apoptosis inducer, in patients with advanced solid tumours. *European Journal of Cancer* 2009; **45**(10): 1764-72.
32. Greeno E, Borazanci E, Gockerman J, Korn R, Saluja A, Von Hoff D. Abstract CT207: Phase I dose escalation and pharmokinetic study of 14-O-phosphonooxymethyltriptolide. *Cancer Research* 2015; **75**(15 Supplement): CT207.
33. Qiu W, Su GH. Challenges and advances in mouse modeling for human pancreatic tumorigenesis and metastasis. *Cancer Metastasis Rev* 2013; **32**(1-2): 83-107.
34. Shannon HE, Fishel ML, Xie J, et al. Longitudinal Bioluminescence Imaging of Primary Versus Abdominal Metastatic Tumor Growth in Orthotopic Pancreatic Tumor Models in NSG Mice. *Pancreas* 2015; **44**(1): 64-75.
35. Weeber F, Ooft SN, Dijkstra KK, Voest EE. Tumor Organoids as a Pre-clinical Cancer Model for Drug Discovery. *Cell Chemical Biology* 2017; **24**(9): 1092-100.
36. Huang L, Holtzinger A, Jagan I, et al. Ductal pancreatic cancer modeling and drug screening using human pluripotent stem cell- and patient-derived tumor organoids. *Nat Med* 2015; **21**(11): 1364-71.
37. Seino T, Kawasaki S, Shimokawa M, et al. Human Pancreatic Tumor Organoids Reveal Loss of Stem Cell Niche Factor Dependence during Disease Progression. *Cell Stem Cell* 2018; **22**(3): 454-67 e6.
38. Boj SF, Hwang CI, Baker LA, et al. Organoid models of human and mouse ductal pancreatic cancer. *Cell* 2015; **160**(1-2): 324-38.
39. Romero-Calvo I, Weber CR, Ray M, et al. Human Organoids Share Structural and Genetic Features with Primary Pancreatic Adenocarcinoma Tumors. *Molecular Cancer Research* 2019; **17**(1): 70-83.
40. Pinto JA, Rolfo C, Raez LE, et al. In silico evaluation of DNA Damage Inducible Transcript 4 gene (DDIT4) as prognostic biomarker in several malignancies. *Scientific Reports* 2017; **7**(1).

41. Park M, Hong J. Roles of NF-κB in Cancer and Inflammatory Diseases and Their Therapeutic Approaches. *Cells* 2016; **5**(2): 15.
42. Liptay S, Weber CK, Ludwig L, Wagner M, Adler G, Schmid RM. Mitogenic and antiapoptotic role of constitutive NF-kappaB/Rel activity in pancreatic cancer. *Int J Cancer* 2003; **105**(6): 735-46.
43. Dolcet X, Llobet D, Pallares J, Matias-Guiu X. NF-kB in development and progression of human cancer. *Virchows Arch* 2005; **446**(5): 475-82.
44. Marquez-Jurado S, Diaz-Colunga J, das Neves RP, et al. Mitochondrial levels determine variability in cell death by modulating apoptotic gene expression. *Nat Commun* 2018; **9**(1): 389.
45. Redza-Dutordoir M, Averill-Bates DA. Activation of apoptosis signalling pathways by reactive oxygen species. *Biochim Biophys Acta* 2016; **1863**(12): 2977-92.
46. Chen BJ. Triptolide, A Novel Immunosuppressive and Anti-Inflammatory Agent Purified from a Chinese Herb Tripterygium Wilfordii Hook F. 2001; **42**(3): 253-65.
47. Torres MP, Rachagani S, Souchek JJ, Mallya K, Johansson SL, Batra SK. Novel Pancreatic Cancer Cell Lines Derived from Genetically Engineered Mouse Models of Spontaneous Pancreatic Adenocarcinoma: Applications in Diagnosis and Therapy. *PLoS ONE* 2013; **8**(11): e80580.
48. Li XJ, Jiang ZZ, Zhang LY. Triptolide: progress on research in pharmacodynamics and toxicology. *J Ethnopharmacol* 2014; **155**(1): 67-79.
49. Liu L, Jiang Z, Liu J, et al. Sex differences in subacute toxicity and hepatic microsomal metabolism of triptolide in rats. *Toxicology* 2010; **271**(1-2): 57-63.

50. Xue X, Gong L, Qi X, et al. Knockout of hepatic P450 reductase aggravates triptolide-induced toxicity. *Toxicol Lett* 2011; **205**(1): 47-54.
51. Fidler JM, An J, Carter BZ, Andreeff M. Preclinical antileukemic activity, toxicology, toxicokinetics and formulation development of triptolide derivative MRx102. *Cancer Chemother Pharmacol* 2014; **73**(5): 961-74.
52. Chen F, Gao X, Shilatifard A. Stably paused genes revealed through inhibition of transcription initiation by the TFIIH inhibitor triptolide. *Genes & Development* 2015; **29**(1): 39-47.
53. Santo L, Vallet S, Hideshima T, et al. AT7519, A novel small molecule multi-cyclin-dependent kinase inhibitor, induces apoptosis in multiple myeloma via GSK-3beta activation and RNA polymerase II inhibition. *Oncogene* 2010; **29**(16): 2325-36.
54. Cai D, Latham VM, Jr., Zhang X, Shapiro GI. Correction: Combined Depletion of Cell Cycle and Transcriptional Cyclin-Dependent Kinase Activities Induces Apoptosis in Cancer Cells. *Cancer Res* 2020; **80**(2): 361.
55. Albensi BC. What Is Nuclear Factor Kappa B (NF-kappa B) Doing in and to the Mitochondrion? *Front Cell Dev Biol* 2019; **7**.
56. Pazarentzos E, Mahul-Mellier AL, Datler C, et al. I kappa B alpha inhibits apoptosis at the outer mitochondrial membrane independently of NF-kappa B retention. *Embo J* 2014; **33**(23): 2814-28.
57. Liu H, Ma Y, Pagliari LJ, et al. TNF-alpha-induced apoptosis of macrophages following inhibition of NF-kappa B: a central role for disruption of mitochondria. *J Immunol* 2004; **172**(3): 1907-15.
58. Adams JM, Cory S. Life-or-death decisions by the Bcl-2 protein family. *Trends Biochem Sci* 2001; **26**(1): 61-6.
59. Vaux DL, Cory S, Adams JM. Bcl-2 gene promotes haemopoietic cell survival and cooperates with c-myc to immortalize pre-B cells. *Nature* 1988; **335**(6189): 440-2.

60. Wolter KG, Hsu YT, Smith CL, Nechushtan A, Xi XG, Youle RJ. Movement of Bax from the cytosol to mitochondria during apoptosis. *J Cell Biol* 1997; **139**(5): 1281-92.
61. Tao Y, Zhang ML, Ma PC, et al. Triptolide inhibits proliferation and induces apoptosis of human melanoma A375 cells. *Asian Pac J Cancer Prev* 2012; **13**(4): 1611-5.
62. Ly JD, Grubb DR, Lawen A. The mitochondrial membrane potential (deltapsi(m)) in apoptosis; an update. *Apoptosis* 2003; **8**(2): 115-28.
63. Gross A, McDonnell JM, Korsmeyer SJ. BCL-2 family members and the mitochondria in apoptosis. *Genes Dev* 1999; **13**(15): 1899-911.
64. Anders S, Huber W. Differential expression analysis for sequence count data. *Genome Biology* 2010; **11**(10): R106.

Figures and Figure Legends

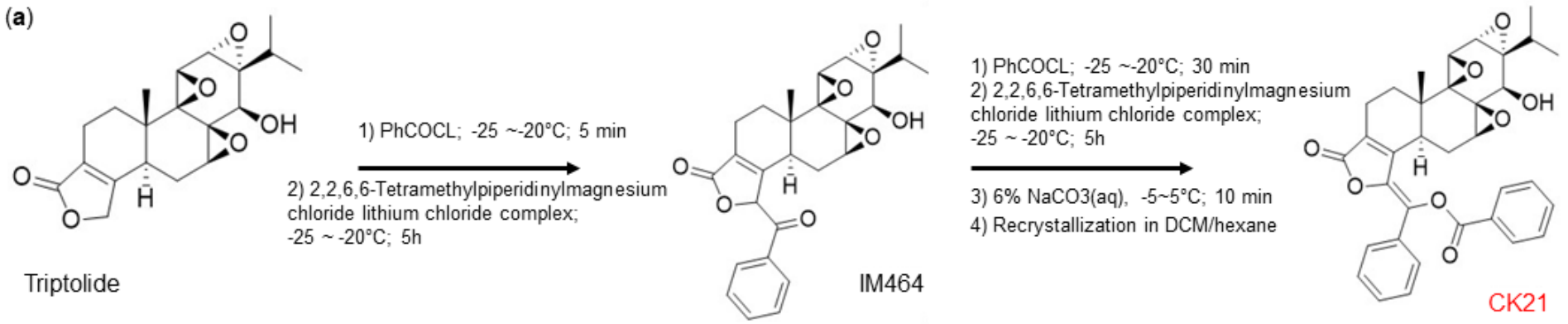

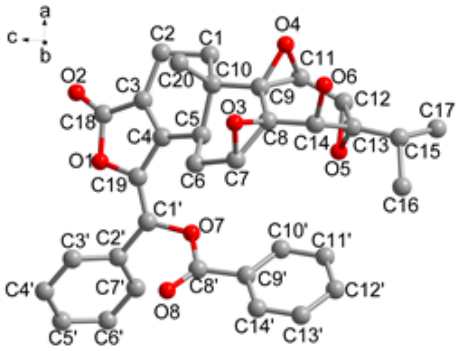

(c)

Components	Function	Content (%)
CK21	API	0.03
Medium chain triglycerides	Oil phase	20
Phospholipids	Emulsifier	2
Glycerol	Isotonic moderator	2.25
DSPE-MPEG2000	Co-emulsifier	0.3
Water for injection	Water phase	77

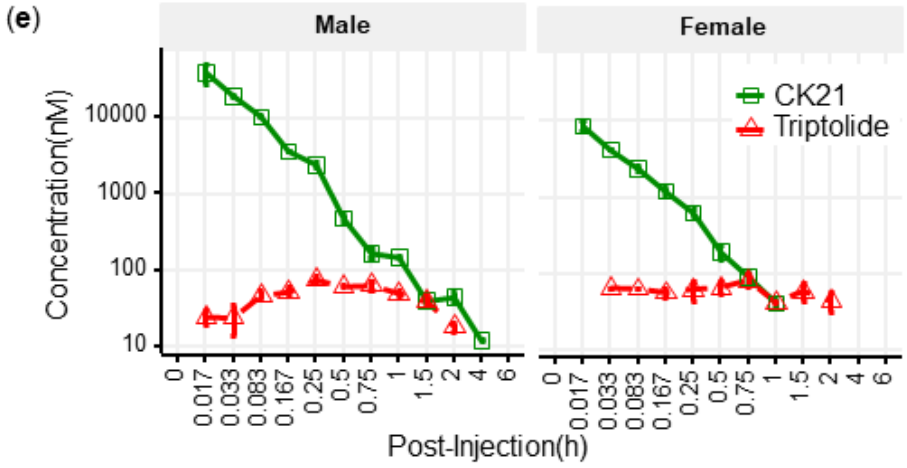

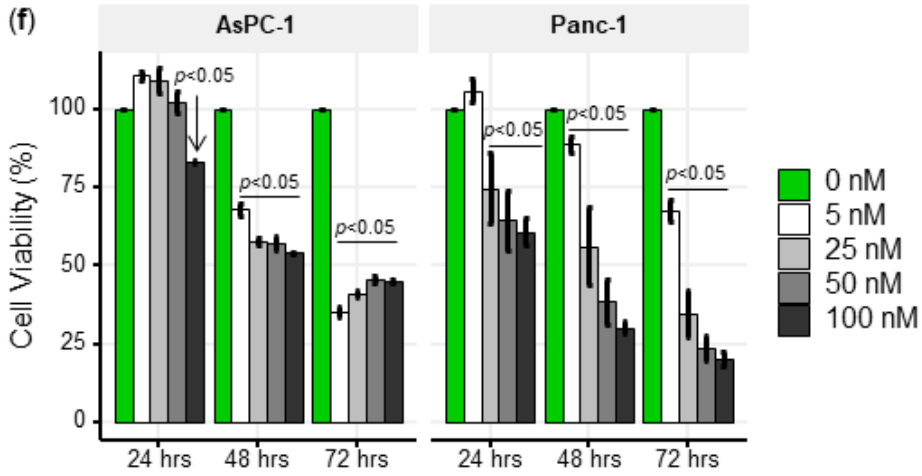

Fig.1. CK21 exhibits a stable release of triptolide *in vivo*. (**a**) Synthesis of compound CK21 as white solid after recrystallization in a mixed organic solvent. Compound structure was characterized by H-NMR, C-NMR and HR-MS. (**b**) Thermal ellipsoid model illustrating the crystal structure of CK21; carbon atoms were shown in gray, and oxygen atoms in red. Hydrogen atoms were omitted for clarity (**c**) Composition and putative function in the CK21 fat emulsion. (**d**) Macroscopic image of the final emulsion product of CK21. (**e**) *In vivo* administration of CK21 into SD rats converted into triptolide. CK21 was injected intravenously into female (1.5 mg/kg) and male (3 mg/kg) rats. (**f**) CK21 inhibited the proliferation of human pancreatic cancer cell lines. Data presented in all the graphs are mean ± standard error. Statistical analysis: Two-way ANOVA (repeated measures) with post-hoc comparison of the means was conducted for (f).

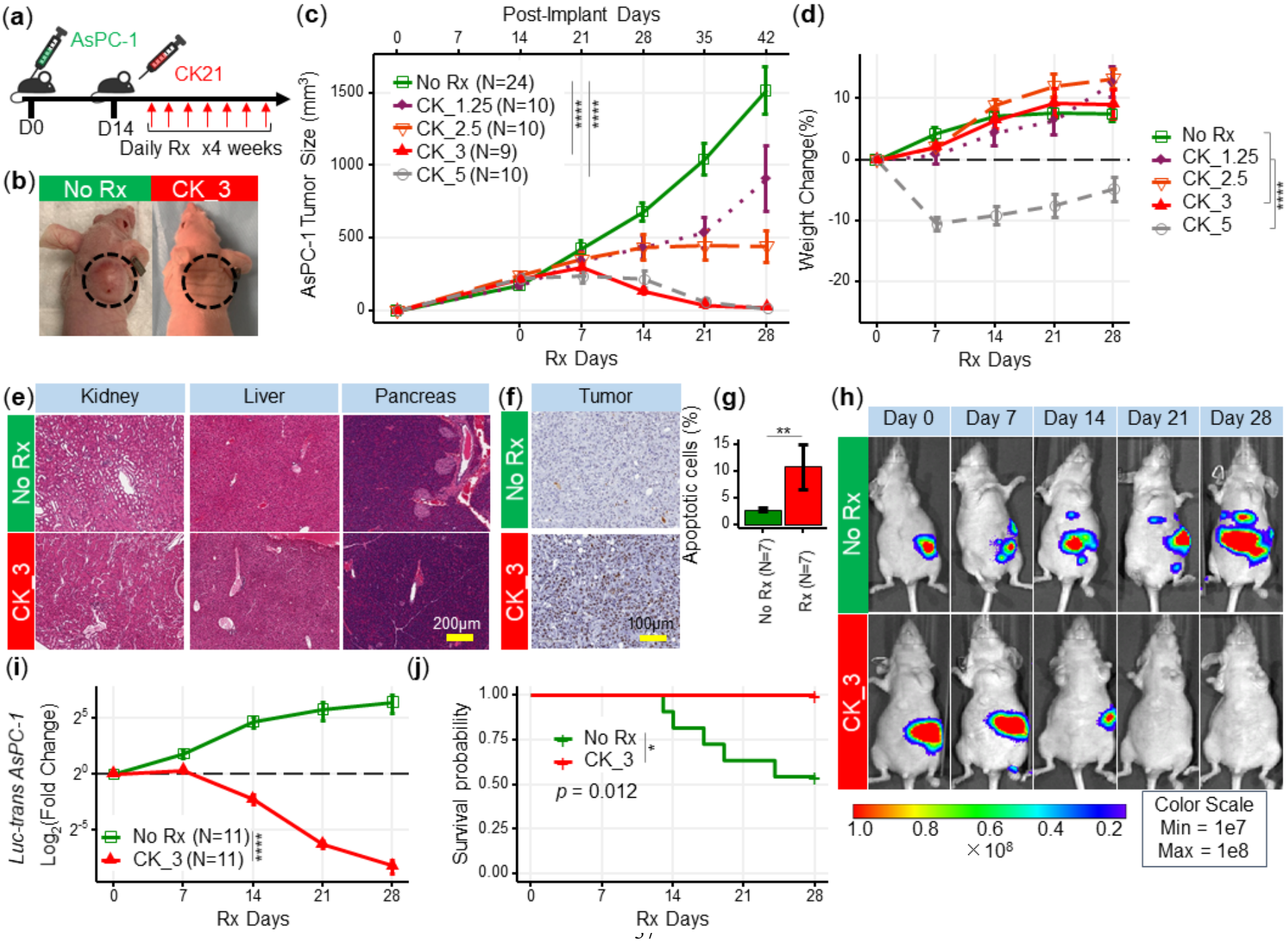
(a)
AsPC-1
CK21
D0
D14
Daily Rx x4 weeks
(b)
No Rx
CK_3
(c)
Post-Implant Days
AsPC-1 Tumor Size (mm³)
No Rx (N=24)
CK_1.25 (N=10)
CK_2.5 (N=10)
CK_3 (N=9)
CK_5 (N=10)
****
****
Rx Days
(d)
Weight Change(%)
No Rx
CK_1.25
CK_2.5
CK_3
CK_5
****
Rx Days
(e)
Kidney
Liver
Pancreas
No Rx
CK_3
200μm
(f)
Tumor
No Rx
CK_3
100μm
(g)
Apoptotic cells (%)
**
No Rx (N=7)
Rx (N=7)
(h)
Day 0
Day 7
Day 14
Day 21
Day 28
No Rx
CK_3
Color Scale
Min = 1e7
Max = 1e8
(i)
Luc-trans AsPC-1
Log2(Fold Change)
No Rx (N=11)
CK_3 (N=11)
****
Rx Days
(j)
Survival probability
No Rx
CK_3
*
p = 0.012
Rx Days

Fig.2. CK21 shows efficacy and minimal toxicity at 3 mg/kg in different *in vivo* animal models. (**a**) Scheme of *in vivo* efficacy studies. Human pancreatic cancer cell line, AsPc-1, was implanted into nude mice and CK21 treatment was initiated ~14 days later, and administered daily for 4 weeks. (**b**) Macroscopic images of tumor-bearing nude mice after receiving CK21 or blank emulsion after 4 weeks treatment. (**c**) AsPC-1 tumor volume after subcutaneous implantation and CK21 or gemcitabine treatment. (**d**) Weight change of the nude mice bearing AsPC-1 and receiving CK21. (**e**) H&E staining of mice organ tissues after CK21 treatment. (**f**) TUNEL staining of tumor tissue and (**g**) percentage of apoptotic cells in AsPC-1 tumor after 2 weeks CK21. (**h**) Bioluminescence images of nude mice bearing intra-pancreatic AsPC-1 and receiving CK21. Color scheme represents the intensity of luminescence reflecting tumor size in each mouse. Mice with higher initial tumor burden was placed into Rx group, and those with lower initial tumor burden into control group. (**i**) Fold change of the luminescence intensity of the nude mice bearing intra-pancreatic AsPC-1. (**j**) Survival curve of mice with orthotopic AsPC-1 tumors receiving CK21 treatment. In all the figures, post-implant days are days after tumor implantation and post-Rx days are days after receiving CK21 treatment. Data presented in all the graphs are mean ± standard error. Statistical analysis: Two-way ANOVA (not repeated measures) with post-hoc comparison of the means of each data set was conducted for all the line graphs except (**i**); For survival curve, Log-rank (Mantel-Cox) test was applied. (* $p< 0.05$, ** $p< 0.01$, *** $p<0.001$, **** $p<0.0001$)

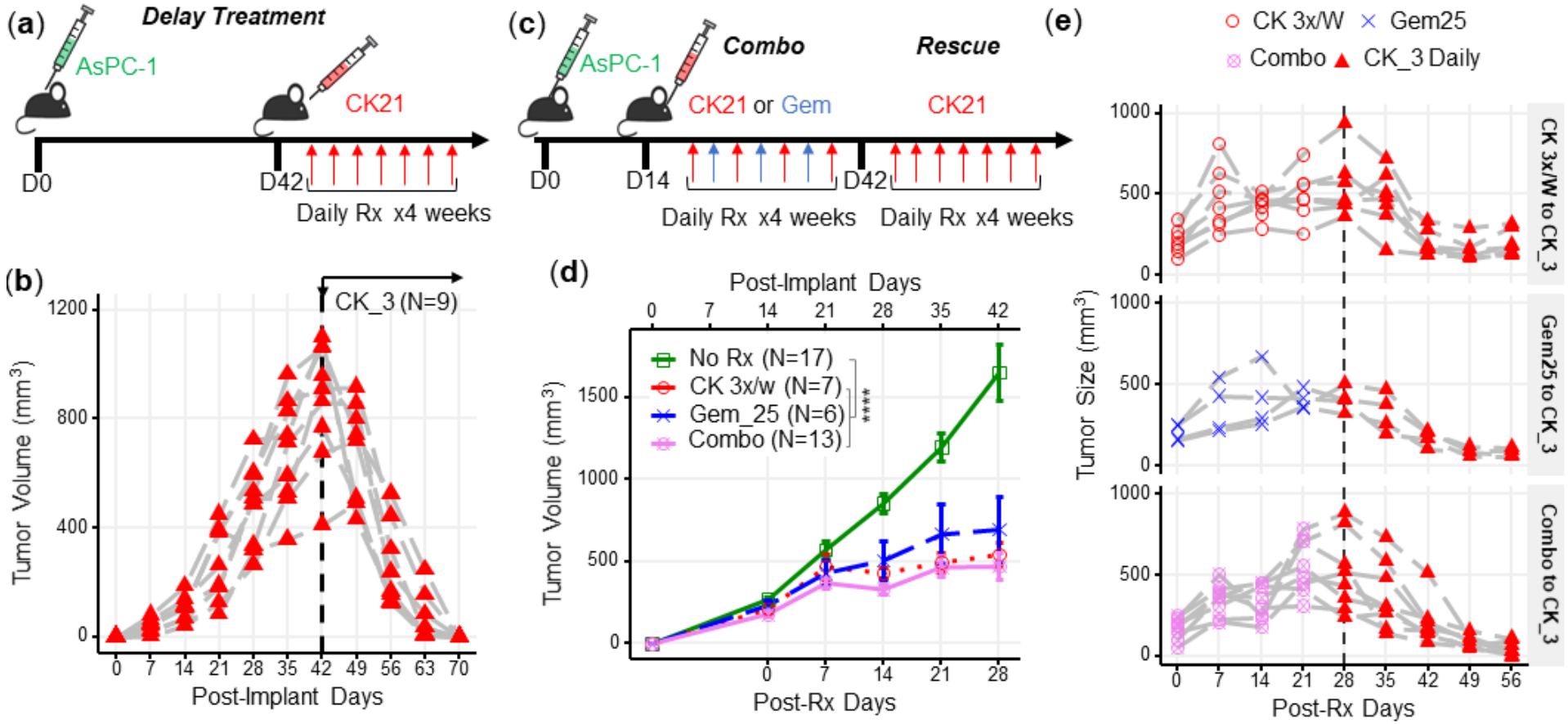

Fig.3. CK21 of 3 mg/kg daily shows efficacy in delay therapy and rescues mice that failed in synergistic therapy. (**a**) Scheme of delayed therapy. Mice received CK21 at 3 mg/kg daily starting on day 42 post-innoculation for 4 weeks. (**b**) Tumor volume during delayed CK21 therapy. (**c**) Scheme of synergistic and rescue therapy. Mice receive CK21 3 mg/kg (3X/week; Mo, We, Fr), gemcitabine at 25 mg/kg (3X/week; Tu, Th, Sa), or both. (**d**) Tumor size during the synergistic therapy of CK21. (**e**) Mice which failed at CK21 or gemcitabine or synergistic therapy were then rescued by switching to CK21 at 3 mg/kg daily, and tumor size monitored. Post-implant days are days after tumor implantation. Post-Rx days are days after receiving CK21 treatment. Data presented in (**d**) are mean ± standard error. Statistical analysis: Two-way ANOVA (not repeated measures) with post-hoc comparison of the means of each data set was conducted for (**d**), (**** p<0.0001). Each line in (**b**) and (**e**) represents a single mouse.

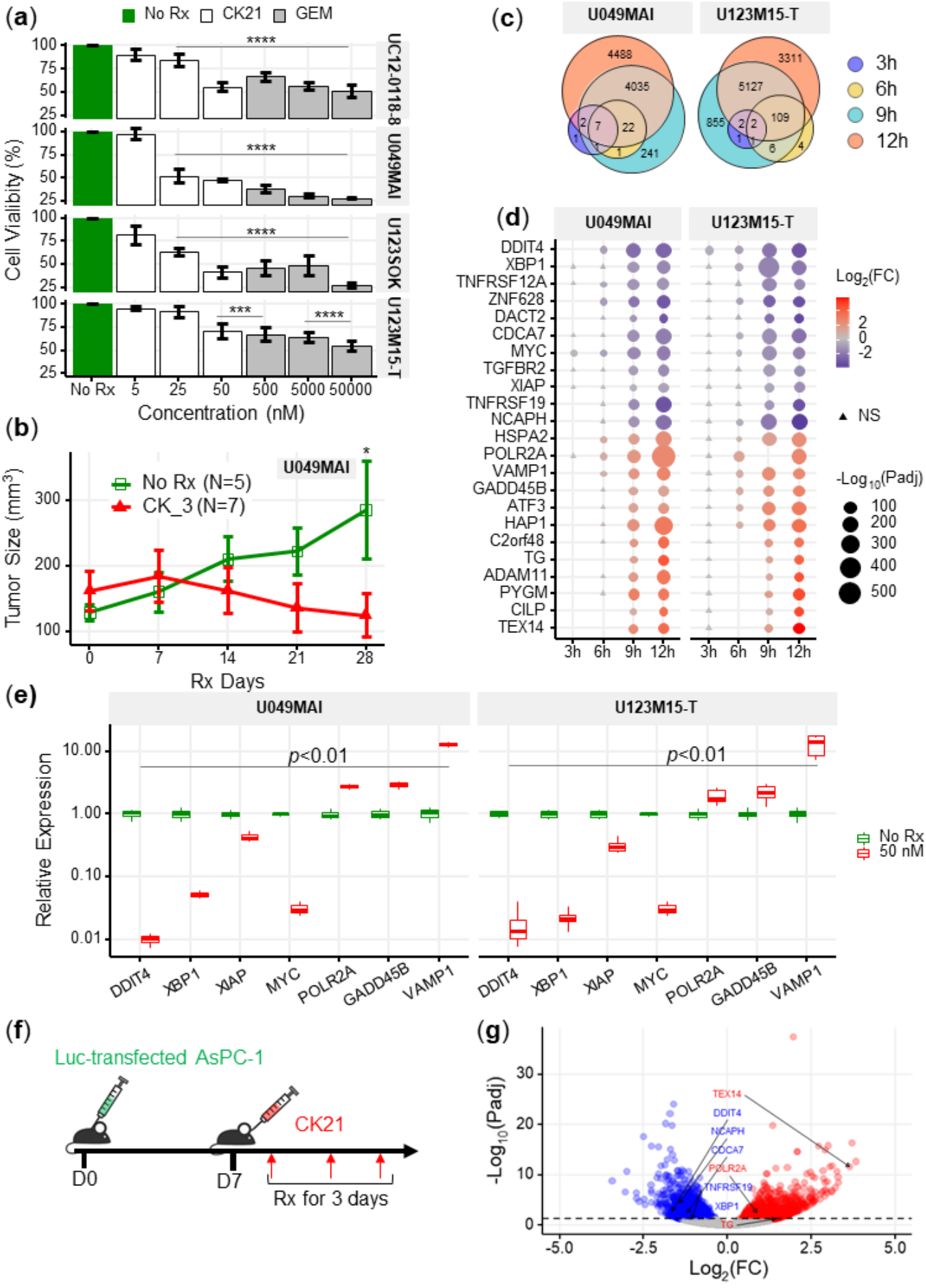

Fig.4. Transcriptome analysis of patient-derived pancreatic tumor organoids after CK21 treatment. (**a**) *In vitro* culture of different organoids with escalating concentrations of CK21 for 72h. Gemcitabine was included as a positive control. (**b**) U049MAI tumor size in nude mice during CK21 treatment. (**c**) Co-expression Venn diagram of differentially expressed genes that were significantly different with CK21 treatment. Size of the circles reflect the total number of differentiate expressed genes (transformed using log2(n+1)). (**d**) Genes of interest showing consistent up or down regulation as treatment time increased. Fold change is color coded where red is upregulation, blue is down regulation. Circle presents the genes had an adjusted p value < 0.05, and triangle presents the genes had an adjusted p value > 0.05. Size of the circle represents the adjusted p values. (**e**) RT-qPCR analysis of gene expression in tumor organoids after CK21 treatment for 24h. (**f**) Scheme of RNA seq using *in vivo* orthotropic AsPC-1 model. (**g**) Volcano plots of statistically significant differentially expressed genes in AsPC-1 tumors after treated with CK21 for three days. Statistical analysis: Two-way ANOVA (not repeated measures) with post-hoc comparison of the means of each time point was conducted for (**a**), and stats was only listed when compared to the No Rx controls. Two-way ANOVA with post-hoc comparison of the means of each time point was conducted for (**b**), Multiple t tests were conducted for (**e**) (** p< 0.01, *** p<0.001, **** p<0.0001)

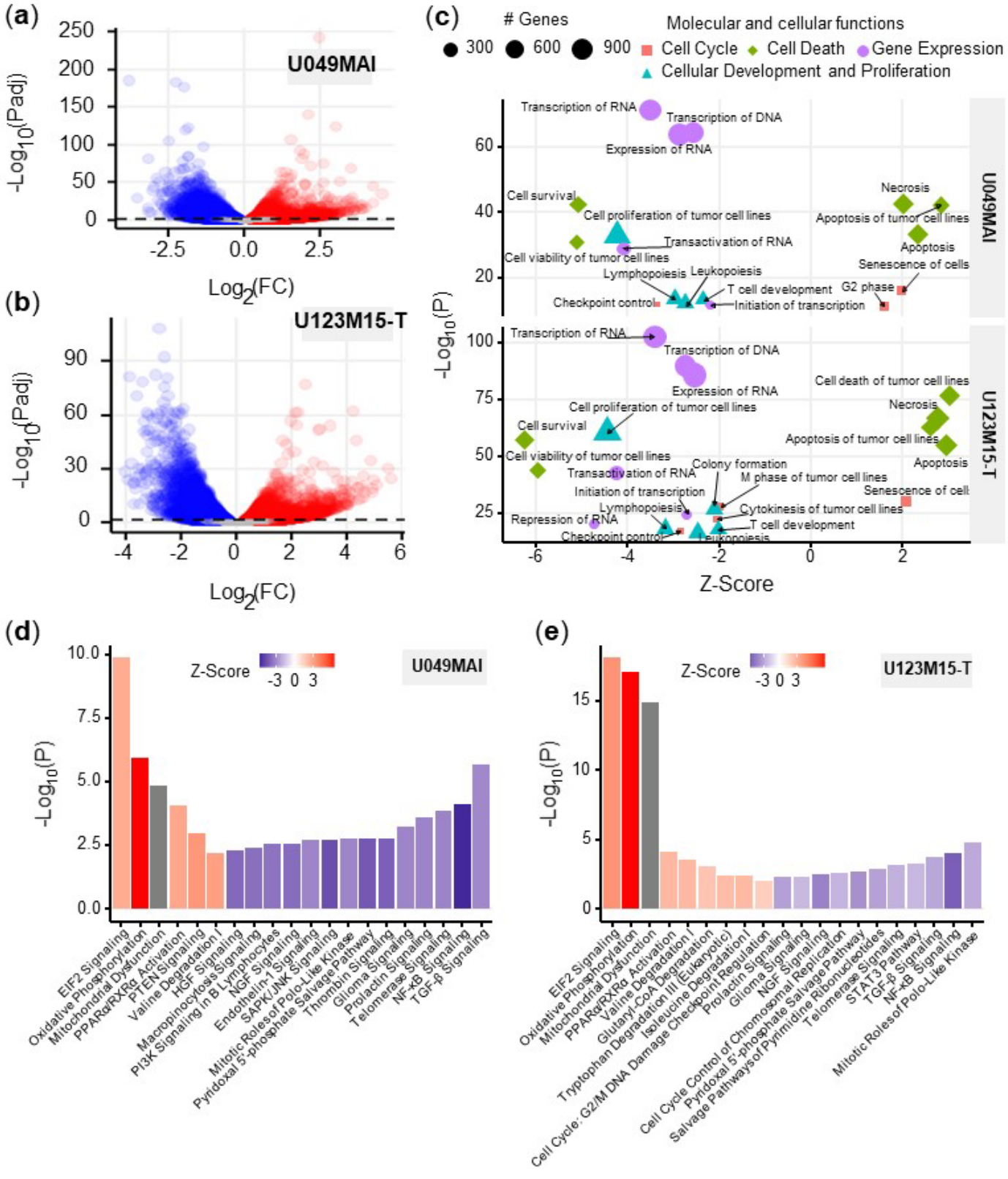

Fig.5. Bioinformatic analysis of the effect of CK21 on patient-derived pancreatic tumor organoids. (**a**) Volcano plots of differentially expressed genes in (**a**) U049MAI and (**b**) U123M15-T after 12 h CK21 treatment (50 nM). Significance cutoff was s $p< 0.05$. Upregulation was colored as red, and downregulation was colored as blue. (**c**) Enrichment of molecular and cellular functions in U049MAI and U123M15-T after CK21 treatment. Size represents gene numbers. Color and shape represent functional groups. Z-score represents the confidence of the prediction, where positive value means upregulation and negative value means downregulation. Canonical pathway enrichment in (**d**) U049MAI and (**e**) U123M15-T after treatment with CK21 at 50 nM. Color represent Z-score where red means upregulation and blue means downregulation. Statistical analysis: Unpaired t-test was conducted for (**c**); Data presented in all the bar graphs are mean ± standard error.

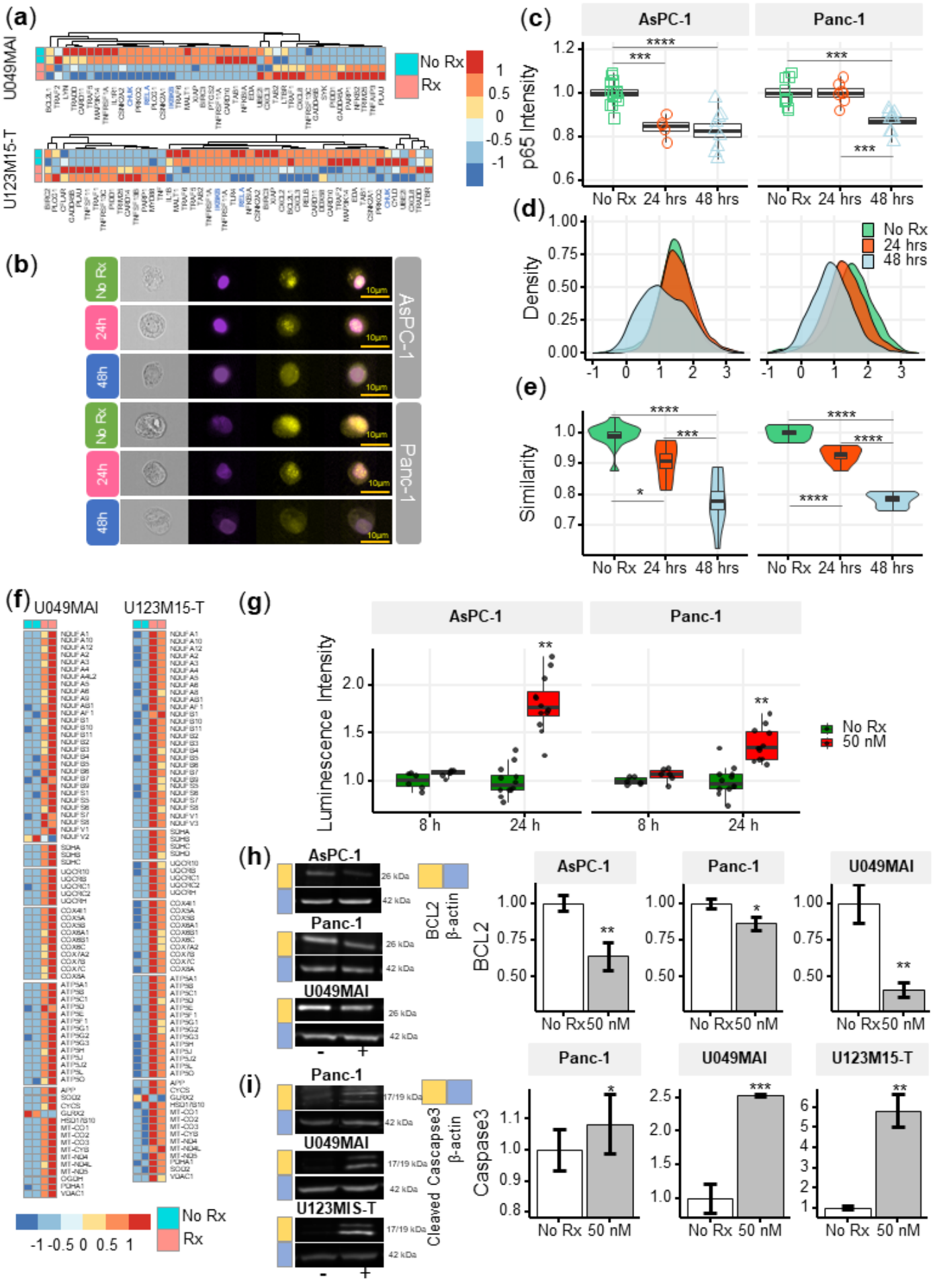

Fig.6. CK21 inhibits NF-κB activation and induces mitochondrial mediated apoptosis. (**a**) Heatmap of the relative expression of genes in the NF-κB pathway in U049MAI and U123M15-T after CK21 treatment. Genes are color coded where red means upregulated, and blue means downregulated. Only statistically significant genes are listed. (**b**) Representative p65 translocation images of AsPC-1 and Panc-1 after treated with CK21 at 50 nM. Nuclei stained as purple, p65 stained as yellow. (**c**) Relative p65 MFI of AsPC-1 and Panc-1 after CK21 (50 nM) treatment. (**d**) Density plots and (**e**) similarity scores of p65 for AsPC-1 and Panc-1. (**f**) Heatmaps of genes involved in oxidative phosphorylation of U049MAI and U123M15-T after CK21 treatment. (**g**) Reactive oxygen species generated after CK21 treatment (8 and 24 hours). Representative blotting images and quantification of (**h**) BCL2 expression and (**i**) cleaved caspase-3 at 24 hours after CK21 treatment. Statistical analysis: One-way ANOVA with post-hoc Tukey comparison of the means of each data set was conducted for (**c**), (**e**); Unpaired T test was conducted at different time points for (**g**), (**h**), (**i**). (* $p< 0.05$, ** $p< 0.01$, *** $p<0.001$, **** $p<0.0001$)

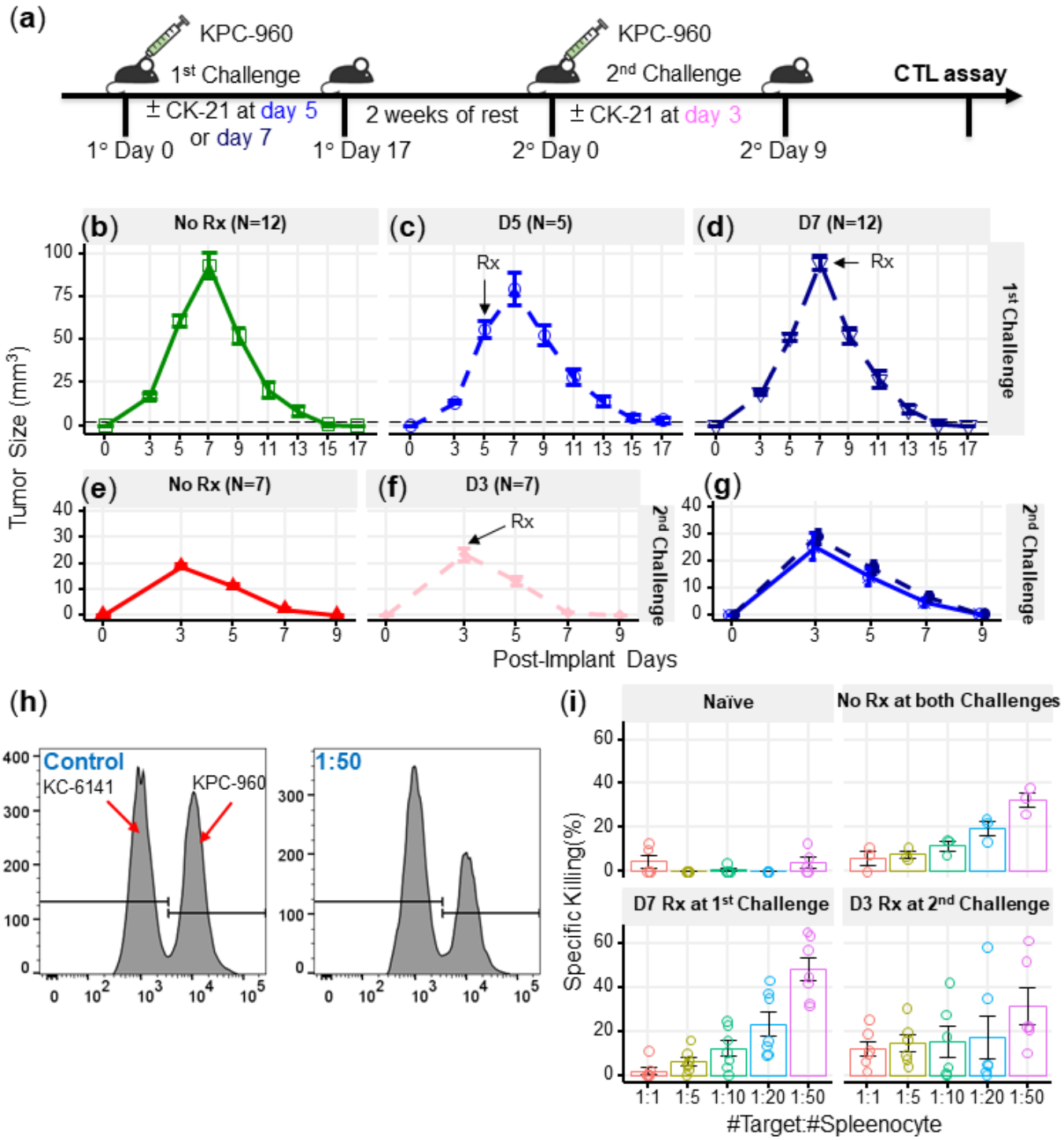

Fig.7. CK21 does not exhibit significant immunosuppression in a spontaneous tumor rejection model. (**a**) Scheme of a subcutaneous model of mouse pancreatic tumor, KPC-960, with CK21 treatment. CK21 was provided at 3 mg/kg daily starting on day 5 or day 7. During secondary challenge, CK21 was provided at 3 mg/kg daily from day 3 post-tumor implantation. Tumor size of mice receiving first challenge (**b**) without any CK21, (**c**) with CK21 starting on day 5. (**d**) or day 7. Tumor size of mice receiving a second challenge (**e**) without any CK21, or (**f**) with CK21 treatment starting on day 3. (**g**) Mice that cleared KPC-960 tumor in (**c**) and (**d**) received a second tumor challenge without any CK21; tumor size were quantified weekly (**h**) Flow plots of CTL assay, another mouse pancreatic tumor, KC-6141, was used as a non-specific target. Quantification of the recovered KPC-960 compared to KC-6141, as a quantification of specific cytotoxic T cell (CTL) killing. (**i**) Specific CTL killing of KPC-960 cells with splenocytes from (**e**), (**f**), (**g**). Splenocytes from naïve mice was included as a negative control. Data presented in all the graphs are mean ± standard error. Statistical analysis: Two-way ANOVA with post-hoc comparison of the means of each time point was conducted for (**b**) and (**e**), (* $p< 0.05$, ** $p< 0.01$, *** $p<0.001$).

Key Resources Table

Reagent	Source	Cat #	RRID
Drugs			
CK21	In house	NA	
Gemcitabine	Actavis	45963-619-59	
Cell lines			
AsPC-1	ATCC	CRL-1682™	CVCL_0152
Luciferase transfected AsPC-1	Indiana University	N/A	
Panc-1	ATCC	CRL-1469™	CVCL_0480
KC-6141	University of Nebraska	N/A	
KPC-960	University of Nebraska	N/A	
KPC-961	University of Nebraska	N/A	
Mice			
B6129SF1/J	Jackson Laboratory	101043	IMSR_JAX:101043
C57BL/6J	Jackson Laboratory	000664	IMSR_JAX:000664
Athymic Nude-Foxn1^{nu}	Envigo		
Cell Culture			
DMEM	ATCC	30-2002™	
RPMI	Quality Biological	112-024-101	
Fetal bovine serum	Atlanta Biologicals	S115OH	
Penicillin streptomycin	Gibco	15140-122	
L-Glutamine	Gibco	25030-081	
DMSO	Sigma	276855	
Trypsin-EDTA	Stemcell	07901	
TrypLE^{TM} express	Gibco	12605-010	
Sodium pyruvate	Gibco	11360-070	
MEM nonessential amino acids	Cellgro	25-025-CL	
2-Mercaptoethanol	Gibco	21985-023	
Organoid Culture			
IntestiCult™ organoid growth medium	Stemcell	6005	
A83-01	Sigma	SML0788	
FGF-10	Sigma	SRP3262	
Gastrin I	Sigma	G9145	
N-acetylcysteine	Sigma	A9165	
Nicotinamide	Sigma	N0636	
B27 supplement	Gibco	17504-044	
Primocine	Invivogen	ant-pm-1	
Y-27632	Tocris	1254	
Matrigel	Corning	356231	
TrypLE^{TM}	Gibco	12605-010	
Multiplex Assay & Flow Cytometry			
CellTiter 96® AQueous one solution	Promega	G3580	
Caspase-3/7 green detection	Thermo Fisher	C10427	
SYTOX® dead cell stain	Thermo Fisher	C10427	

CFSE cell proliferation kit	Thermo Fisher	C34554	
ACK lysing buffer	Quality Biological	118-156-101	
ROS-Glo™ H_2O_2 assay	Promega	G8820	
Western Blotting			
NuPAGE™ 10% Bis-Tris gel	Invitrogen	NP0301BOX	
NuPAGE® MES SDS running buffer	Novex	NP002	
NuPAGE® MOPS SDS running buffer	Novex	NP001	
NuPAGE® transfer buffer	Novex	NP0006-1	
NuPAGE® LDS sample reducing agent	Invitrogen	NP0007	
NuPAGE® sample buffer	Invitrogen	NP0009	
NuPAGE™® antioxidant	Invitrogen	NP0005	
TBS Tween™-20 buffer	Thermo Scientific	28360	
Invitrolon™ PVDF filter paper	Novex	LC2005	
PageRuler prestained protein ladder	Thermo Scientific	26616	
Methanol	Fisher Scientific	A452-4	
Pierce™ protease&phosphatase inhibitor	Thermo Scientific	A32959	
Bovine serum albumin	Sigma	A7906	
SuperSignal™ west pico PLUS	Thermo Scientific	34579	
Pierce™ bradford assay kit	Thermo Scientific	23246	
Antibodies			
Anti-beta actin	Abcam	ab8227	AB_2305186
Recombinant anti-REDD-1/DDIT4	Abcam	ab191871	
Anti-Caspase-3	Abcam	ab13847	AB_443014
Recombinant anti- BCL2	Abcam	ab182858	AB_2715467
Goat anti-rabbit IgG H&L	Abcam	ab205718	AB_2819160
4',6-Diamidino-2-Phenylindole, Dilactate	Biolegend	422801	
Phospho-NF□B p65, PE, eBioscience™	Invitrogen	12986342	AB_2572751
RT-qPCR			
PowerUp™ SYBR™ green master mix	Applied Biosystem	A25742	
High capacity cDNA reverse transcription	Applied Biosystem	4368814	
Bioluminescence Imaging			
D-Luciferin potassium salt	Perkin Elmer	122799	
PBS	GenClone	25-508	
RNA-Seq			
Cell recovery solution	Corning	354253	
RNeasy® Plus Mini Kit	Qiangen	74124	
DNase I recombinant	Roche	04536282001	

831

Fig.s1. IC50 (μM) of triptolide (TP) or CK21 for different cancer cell lines and human fibroblasts in an in vitro cell viability assay.

Compound	HFL-1	SK-OV-3	PC-3	AsPC-1 (Round1)	AsPC-1 (Round2)
TP	0.02	0.21	0.013	0.018	0.027
CK21	0.044	0.04	0.035	0.022	0.056

HFL-1: human fetal lung fibroblast cell line; SK-OV-3: ovarian adenocarcinoma; PC-3: prostatic adenocarcinoma; AsPC-1: pancreatic adenocarcinoma

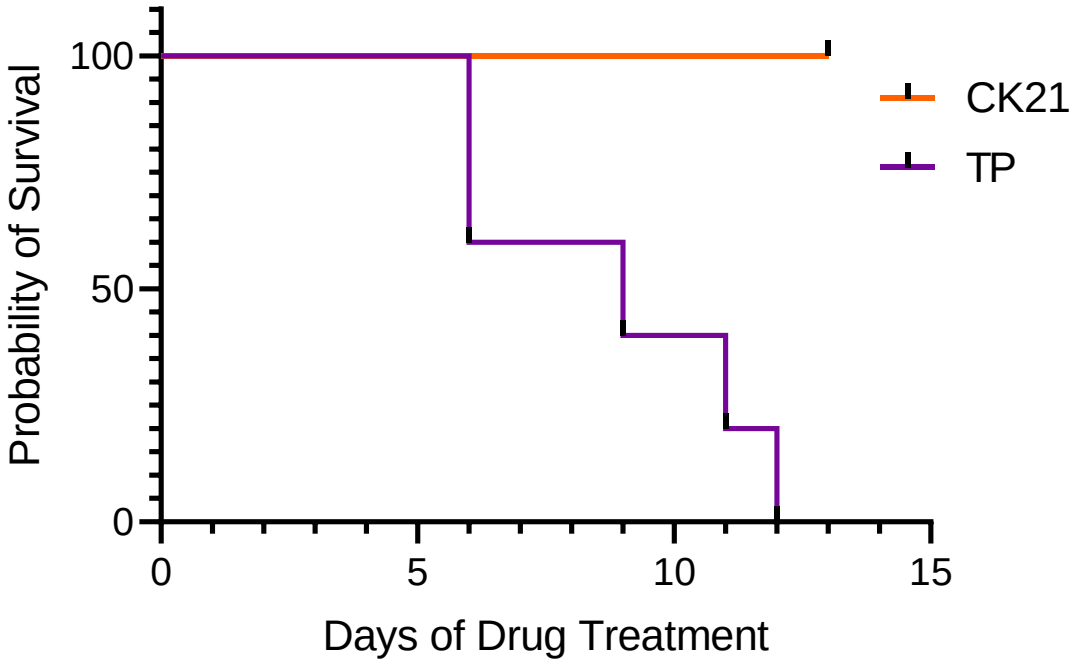

Fig.s2. Survival curve of mice receiving CK21 at 5mg/kg or triptolide (TP) at 0.25 mg/kg.

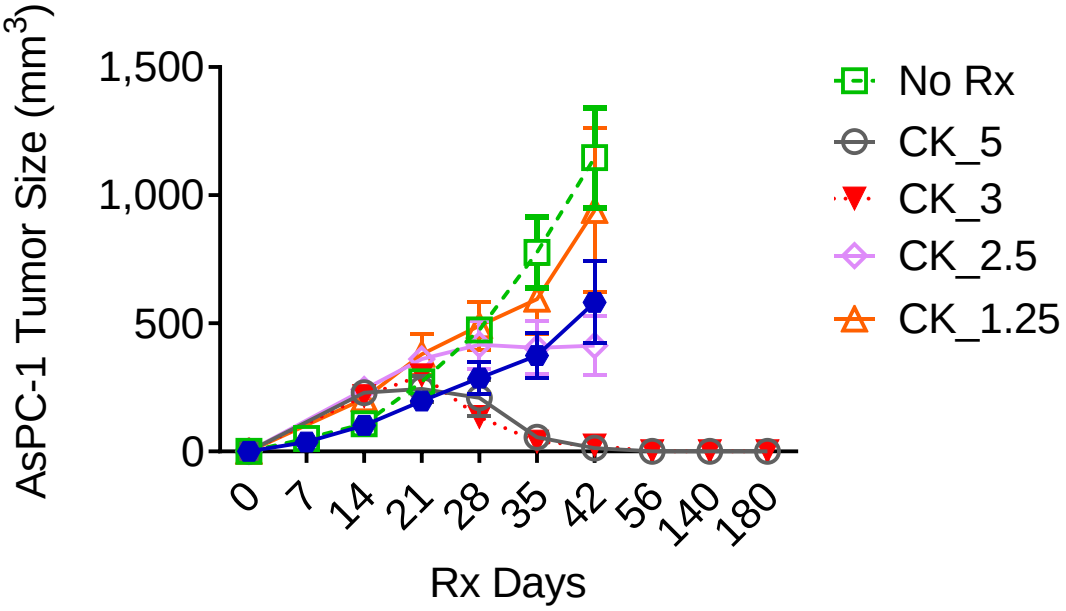

Fig.s3. AsPC-1 subcutaneous tumors showed no tumor relapse after treated with CK21 at 5 or 3 mg/kg.

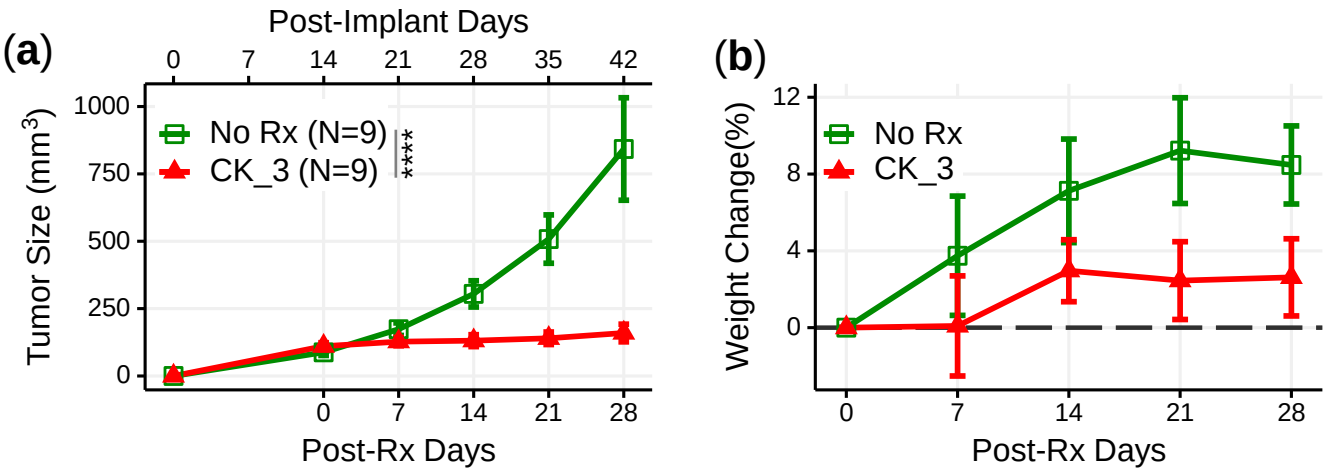

Fig.s4. CK21 inhibited growth of Panc-1 tumors in a subcutaneous xenograft model. (a) Tumor growth with CK21 treatment at 3 mg/kg daily for 28 days. (b) Weight change of mice during Ck21 treatment.

Organoids	Patient #	Mutations	Origin	Adjuvant Therapy	Sex
UC12-0118-4	1	KRAS_G12R TP53_F134L	PDX (derived from PDAC)	Gemcitabine; FOLFIRINOX	F
UC12-0118-8	2	KRAS_G12R TP53_F270L	PDX (derived from PDAC)	FOLFIRINOX (no irinotecan); Gemcitabine/Abraxane	M
U123	6	KRAS_G12D TP53_G245S	Primary(PDAC)	Gemcitabine; Gemcitabine/Abraxane	M
U114	7	KRAS_G12D TP53-chr17_7578176_C->T	Primary(PDAC)	Gemcitabine; Gemcitabine/Abraxane	M

Fig.s5 . Essential information on the pancreatic tumor organoids used in this study. Details of organoids from Patient# 1, 2, 6 and 7 are provided in reference 39 (Romero-Calvo et al., Molecular Cancer Research 2019)

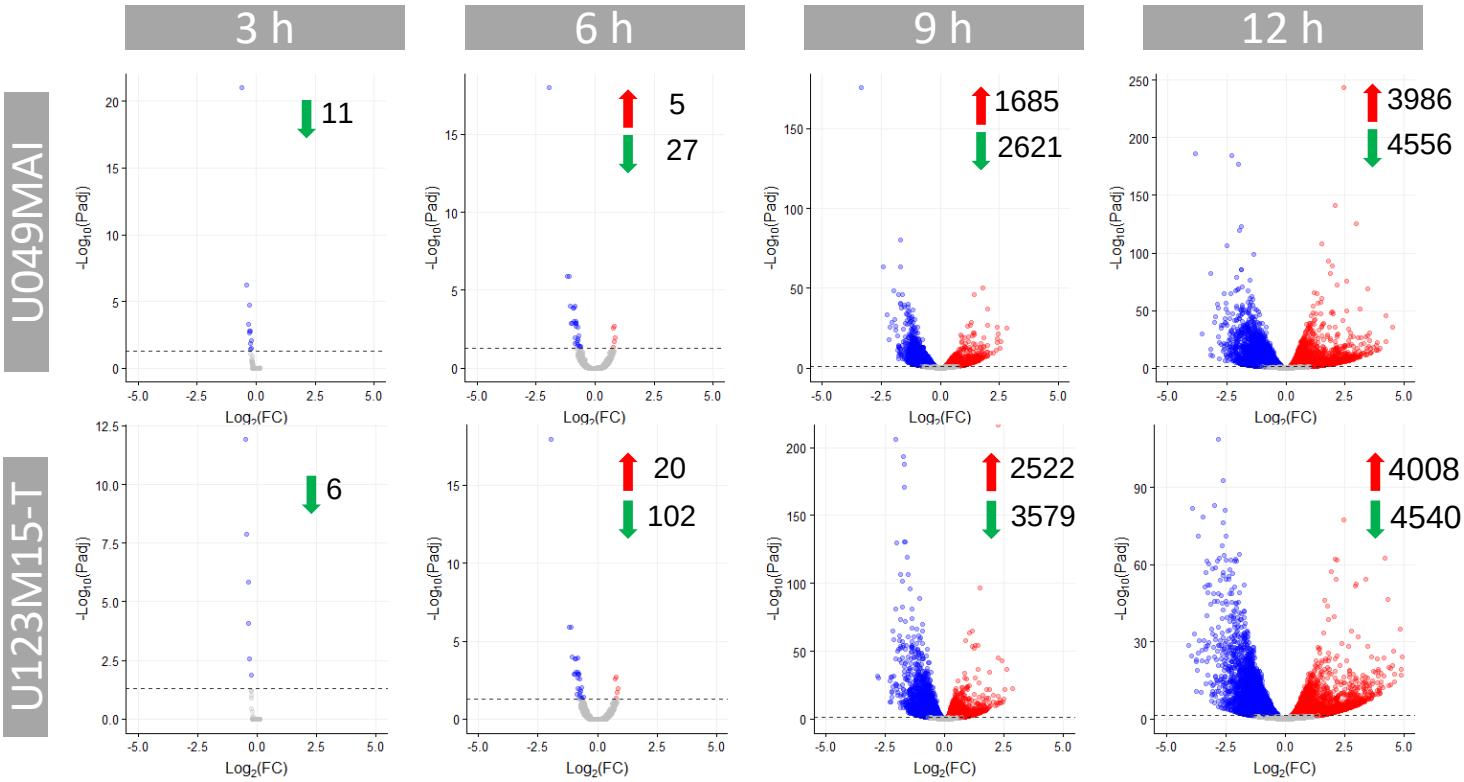

Fig.s6. Volcano plots highlighting differentially expressed genes by U049MAI and U123m15-T respectively after 3h, 6h, 9h and 12 h of CK21 (50 nM) treatment.

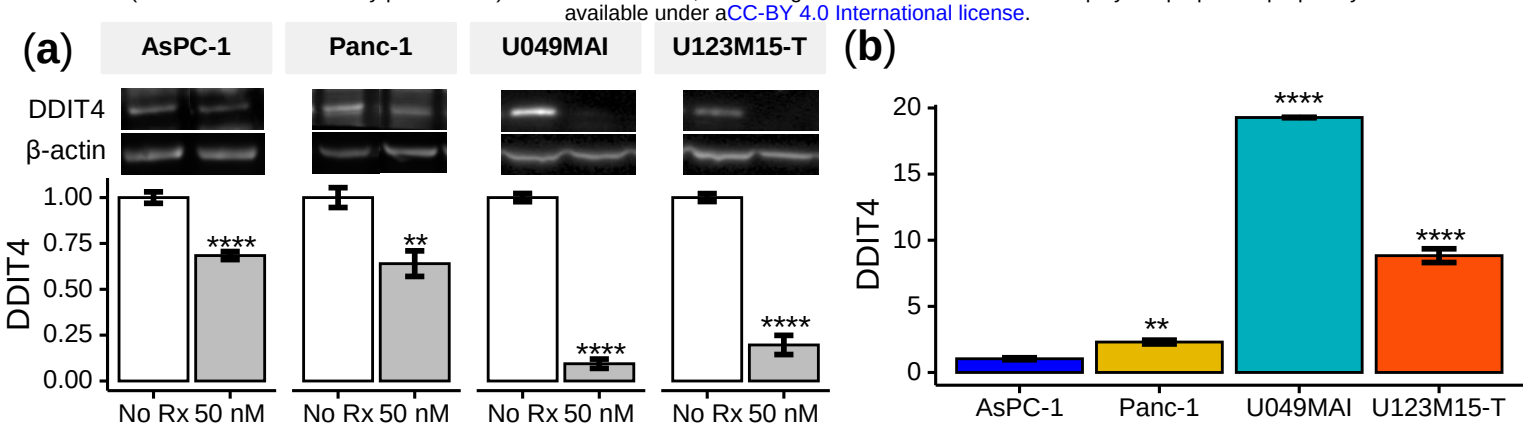

Fig.s7. (a) CK21 (50 mM) reduced the expression of DDIT4 in AsPC-1, Panc-1, U049MAI, and U123M15-T after 24 hours of culture. (b) Baseline expression of DDIT4 in different tumor cells (without CK21 treatment).

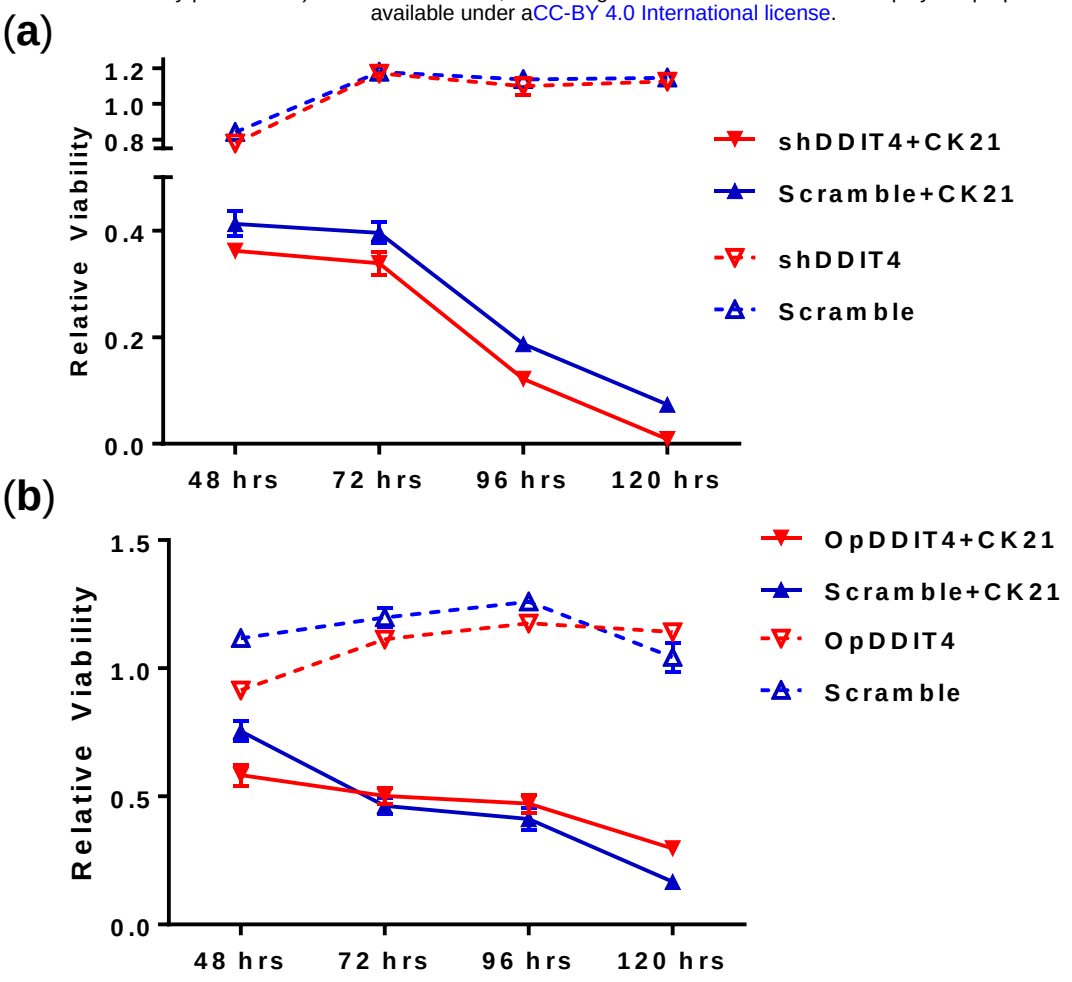

Fig.s8 (a) knockdown of DDIT4 in Panc-1 did not alter response to CK21 (50 nM). (b) AsPC-1 overexpression of DDIT4 did not alter response to CK21 (50 nM).

(a)

Murine PDAC cells	Confirmed mutations	Mice model	Host mice
KC-6141	$Kras^{G12D}$	KC	B6
KPC-961	$Kras^{G12D}$ $Trp53^{R172H}$	KPC	B6×129

(b)

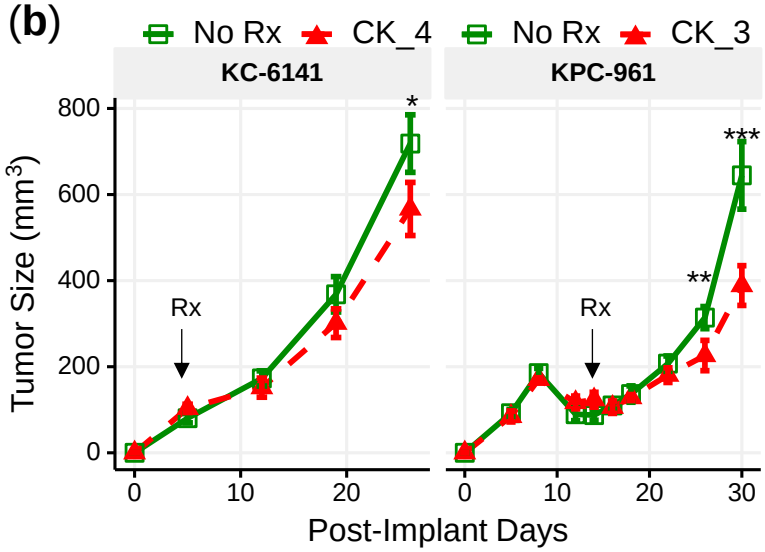

Fig.s9 (a) Information for murine pancreatic cancer cell lines. (b) Tumor size of KC-6141 and KPC-961 after subcutaneous implantation. CK21 given at 4 mg/kg/day for KC-6141 and 3 mg/kg/day for KPC-961 resulted in modest inhibition of tumor growth.

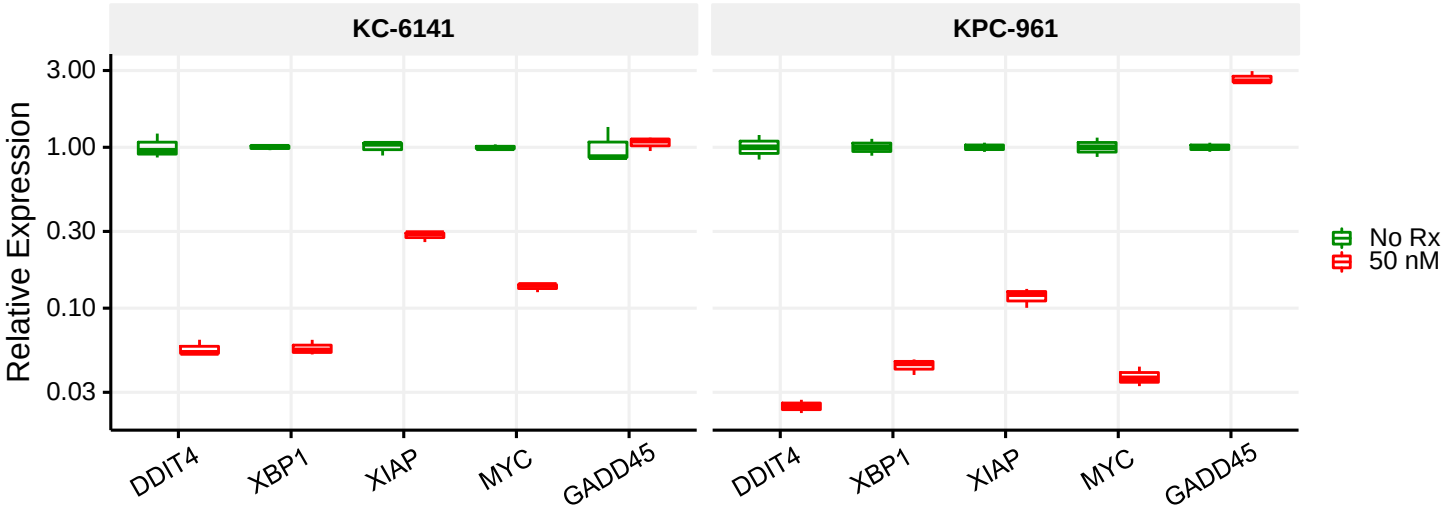

Fig.s10 RT-qPCR analysis of differentially expressed genes by two mice pancreatic tumor cell lines after CK21 treatment at 50 nM for 24h.

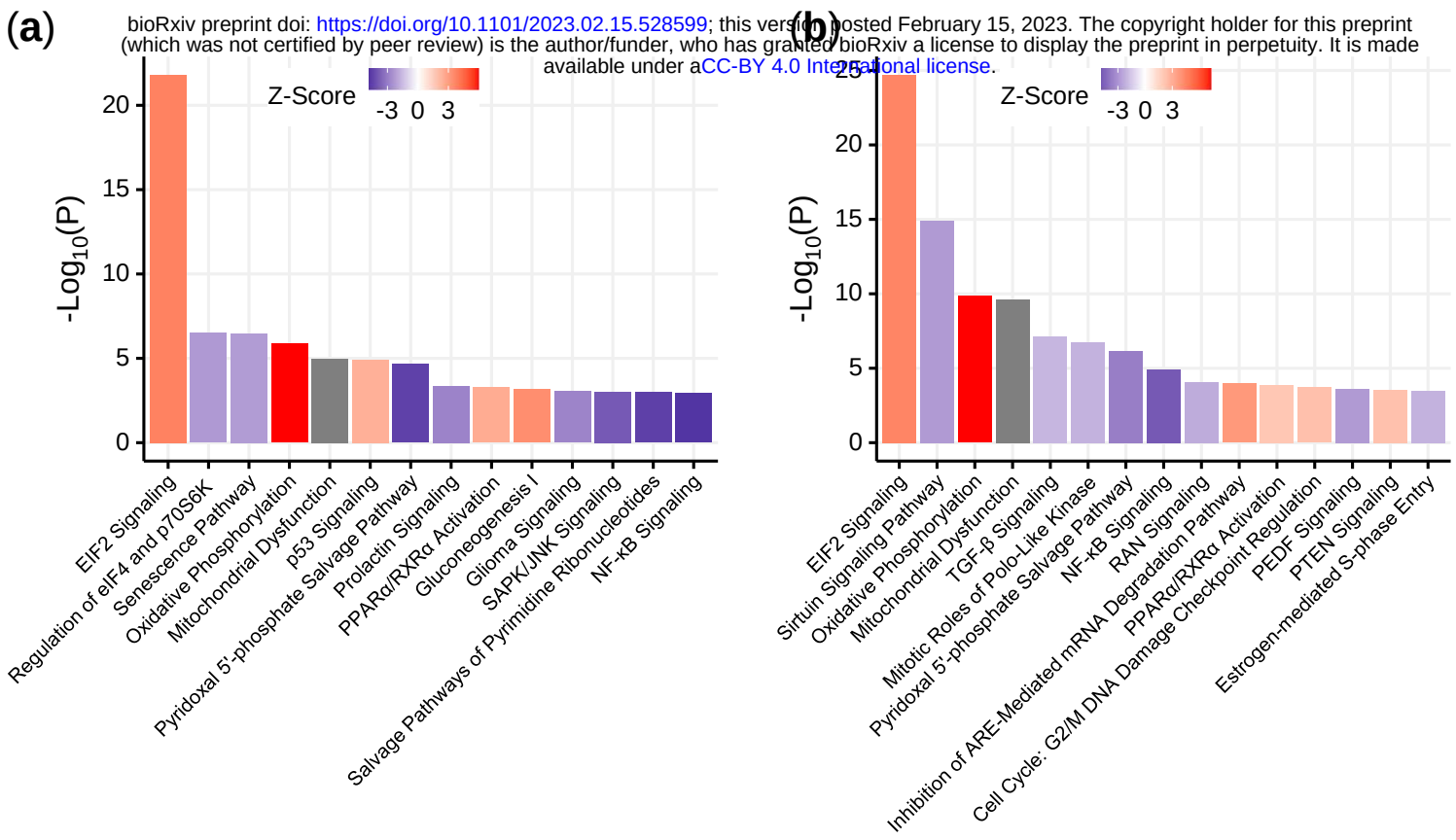

Fig.s11 Pathway enrichment of U049MAI and U123m15-T after treatment with CK21 (50 nM) for 9 hours. Top pathways for (a) U049MAI and (b) U123M15-T

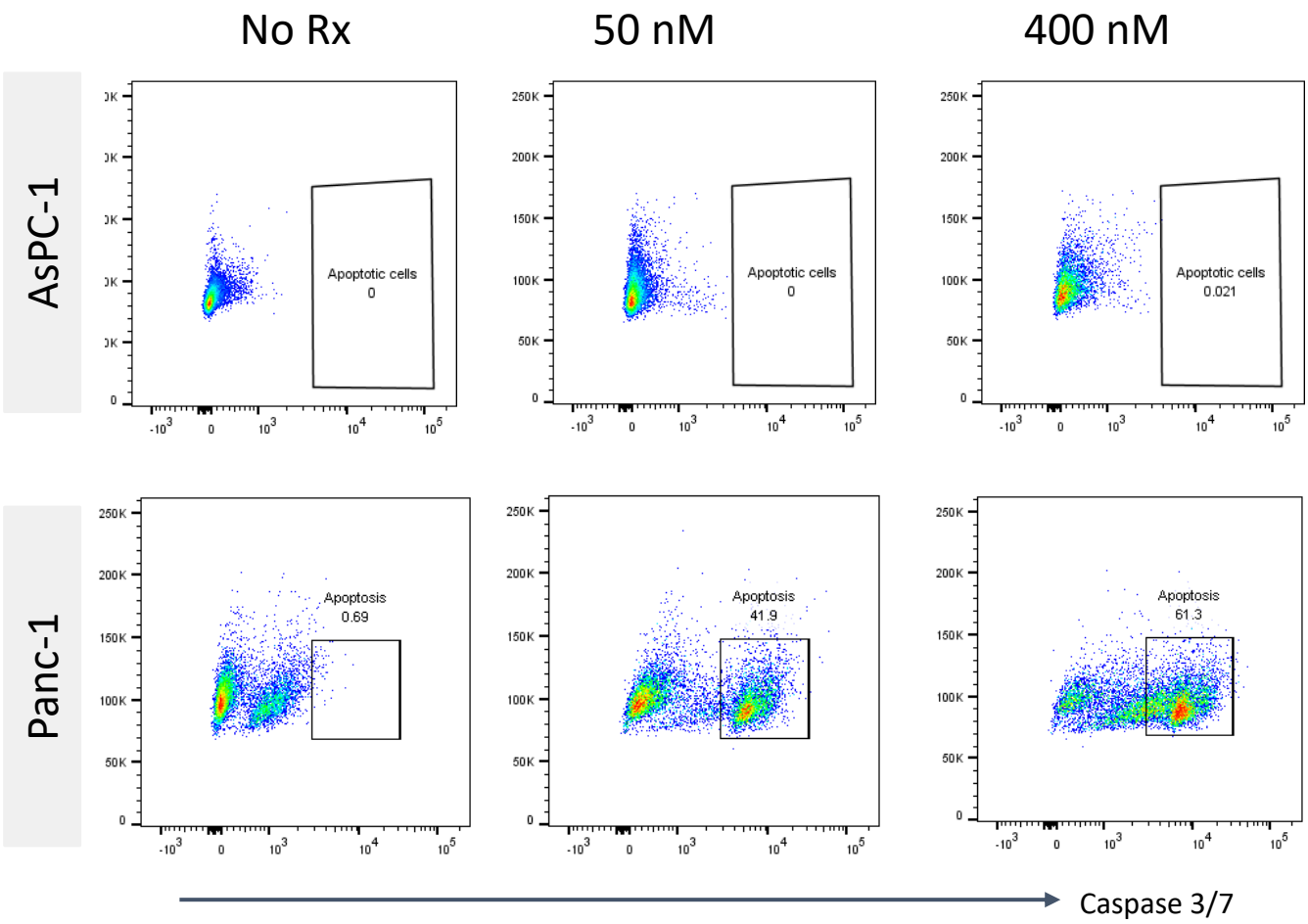

Fig.s12 Flow plots illustrating active Caspase 3/7 expression in AsPC-1 and Panc-1 treated with CK21 (50 and 400 mM) for 24 hours.

Study ID	Species	Route	Dose	Observation	
Acute MTD (single dose[α])	Rats (20/sex)	IV infusion (20 mL/kg/hour)	1.5, 3 or 6 mg/kg	Mortality (five females at 6 mg/kg)	Liver & kidney toxicity[γ]
Toxicity and Toxicokinetic (daily dose[β])	Rats (88 males; 100 females)	IV infusion (20 mL/kg/hour)	1, 2 or 4 mg/kg (male); 0.5, 1 or 2 mg/kg (female)	well tolerated for both male and female[δ]	
Acute MTD (single dose on days 1,3,5[α])	Beagle Dogs (4/sex)	IV infusion (30 min)	0.2, 0.4, and 0.8 mg/kg	well tolerated for both male and female[ε]	

[α] Single CK21 dose followed by a 14-day observation and recovery period.
[β] 28 consecutive days of CK21 treatment followed by a 28-day observation and recovery period.
[γ] Increases of alanine aminotransferase, aspartate aminotransferase, total bilirubin, and alkaline phosphatase correlated with potential hepatotoxicity. Increases of urea and creatinine correlated with potential kidney toxicity.
[δ] No treatment-related mortality, and no adverse effects in clinical signs: body weight, food consumption, ophthalmology, clinical pathology, organ weight of thymus, ovaries, uterus and spleen, gross findings of enlarged spleen and microscopic changes in bone marrow (sternum and femur), ovaries, spleen, liver, kidneys, lymph nodes (mandibular and mesenteric), and thymus.
[ε] No test CK21-related effects on food consumption, hematology, coagulation, serum chemistry or macroscopic findings at necropsy.

Fig.s13 Safety profile of CK21. Acute maximum tolerated dose (MTD) studies, toxicity and toxicokinetic studies on rats and beagle dogs.

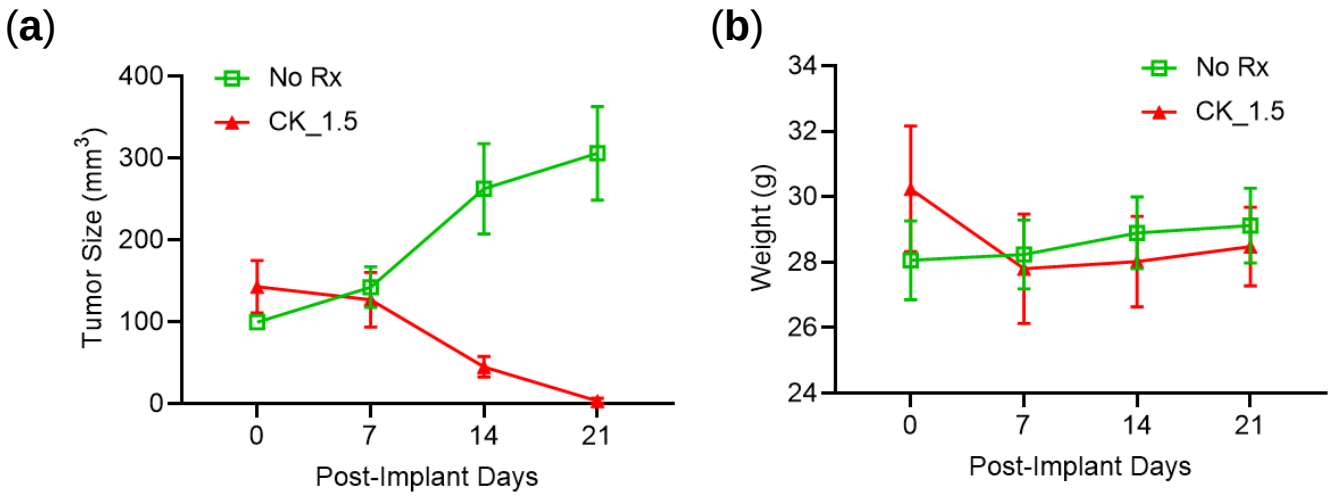

Fig.s14 Male mice with AsPC-1 tumors responded to CK21. (a) Subcutaneous AsPC-1 tumor in male mice after CK21 treatment at 1.5 mg/kg. (b) Male mice weight during CK21 treatment. (N=5 for each experimental group)

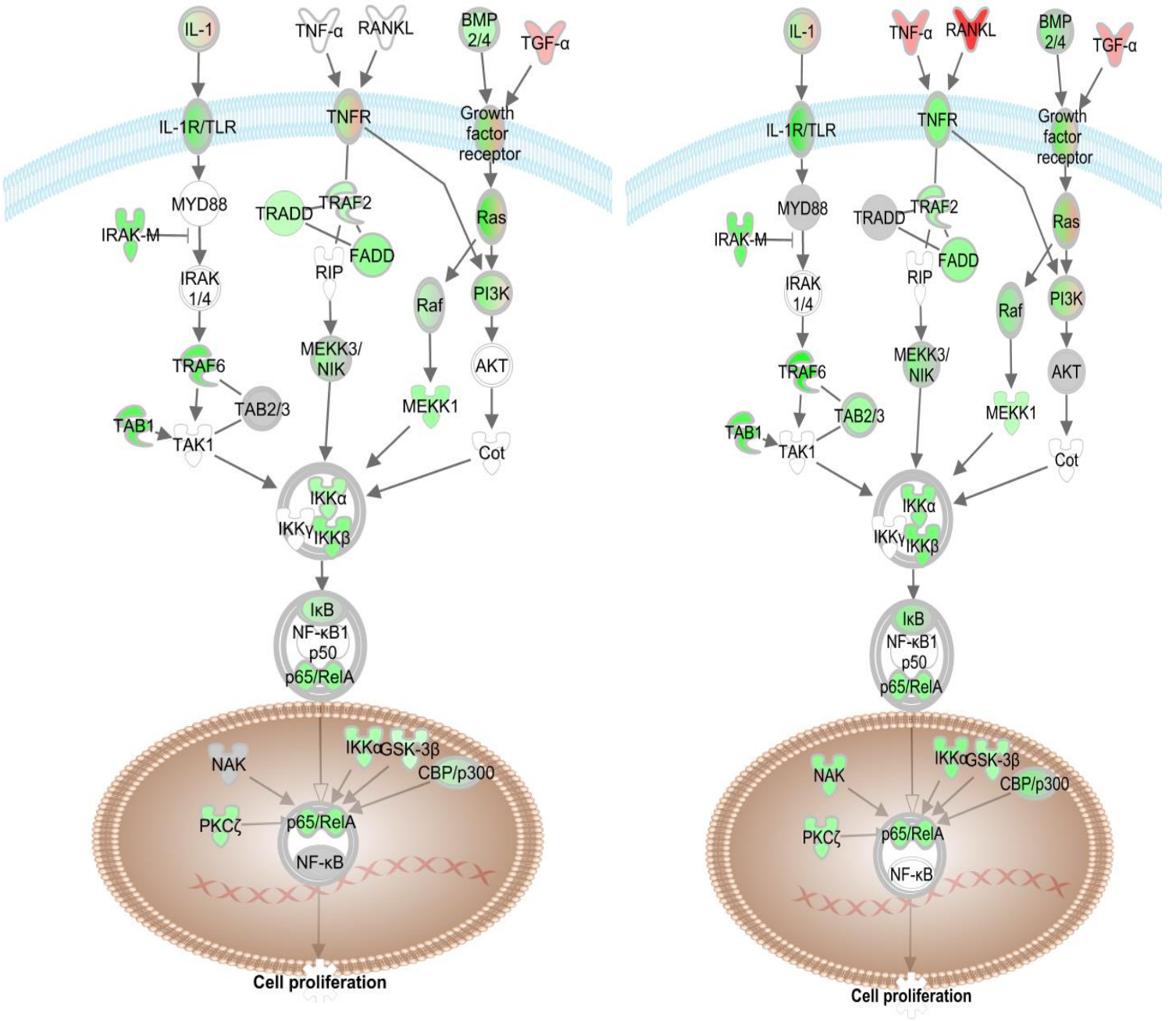

Fig.s15 Key regulators in NF-κB canonical signaling pathway are significantly downregulated in (a) U049MAI and (b) U123m15-T after treatment with CK21 (50 nM) for 12 hours. Green represent downregulation and red represent upregulation by IPA analysis.